Tang, Yongqi; Lv, Wei; Wang, Yao; Chen, Hong; Li, Yongdan; Wang, Can; Xu, Guifeng

Research progress of Co and Mn-based catalysts for the oxidation of 5-hydroxymethylfurfural

Published in:
ChemCatChem

DOI:
10.1002/cctc.202301376

Published: 22/04/2024

Document Version
Peer-reviewed accepted author manuscript, also known as Final accepted manuscript or Post-print

Research progress of Co and Mn-based catalysts for the oxidation of 5-hydroxymethylfurfural

Yongqi Tang [a], Wei Lv [a], Yao Wang [a], Hong Chen [a,*], Yongdan Li [b,c], Can Wang [a], Guifeng Xu [a]

[a] School of Environmental Science and Engineering, Tianjin University, Tianjin 300072, China

[b] Collaborative Innovation Center of Chemical Science and Engineering, Tianjin Key Laboratory of Applied Catalysis Science and Technology, State Key Laboratory of Chemical Engineering, School of Chemical Engineering, Tianjin University, Tianjin 300072, China

[c] Department of Chemical and Metallurgical Engineering, School of Chemical Engineering, Aalto University, Kemistintie 1, Espoo FI-00076, Finland

* Corresponding author. E-mail address: chenhong_0405@tju.edu.cn (H. Chen).

Abstract

Biomass is a renewable energy source abundantly available in nature. Their degradation by chemical or biological means produces various transition compounds. These transition compounds can be further transformed into valuable chemicals and biofuels that exhibit a wide range of applications and benefits. Recently, there has been a significant focus on this research area. Among the transition compounds, 5-hydroxymethylfurfural (HMF), derived from the degradation of hexose, is an important biomass-based platform compound that has hydroxymethyl and aldehyde functional groups in its molecular structure. This study reviews the recent progress in the transition metal-catalysed conversion of HMF using Co and Mn to generate high-value-added downstream products. Furthermore, the active components, the carbon supporter, the reaction mechanism, the oxidants and the reaction conditions of the catalysts are discussed in detail. The oxidation of HMF deserves further research as an important and complete value-added process for generating biomass-based valuable chemicals.

Keywords: Biomass; hydroxymethylfurfural (HMF); transition metal catalyst; redox reaction.

1. Introduction

The depletion of natural resources, increase in greenhouse gas emissions, and the global shift towards decarbonisation and bioeconomy have led to a surge of interest in the conversion of biomass into high-value chemicals and functional materials. Improving the utilisation of biomass is vital for achieving sustainable development. Biomass energy sources are mainly classified into forestry residues, crop residues, agro-processing wastes, livestock manure, and municipal waste. Among them, lignocellulosic biomass resources, such as cellulose (40–50%), hemicellulose (20–30%), and lignin (10– 25%), are renewable biomass resources that exist abundantly on the earth. Oxidation of lignocellulosic platform molecules has been identified as an effective process to obtain value-added chemicals.[1] Four key platform molecules, including glucose, 5-hydroxymethylfurfural (HMF), as well as furfural and acetyl propionic acid, have been identified as downstream high-value compounds.[2, 3] Cellulose has β -1,4-bonded anhydrous glucose units[4], which can be converted to important biobased platform compounds such as glucose (hydrolysis), fructose (in situ isomerisation) and HMF (dehydration).[5-7] The multifunctionality of HMF, as a promising molecule for a wide range of biomass-based platform compounds,[1,8, 9] is attributed to the hydroxyl, aldehyde, and furan ring structures, as illustrated in Fig 1. The structure of these functional groups imparts various chemical activities. HMF can be oxidised to 2,5-furandicarboxylic acid (FDCA)[10, 11], 2,5-diformylfuran (DFF)[12], and maleic anhydride (MAH)[13]. Furthermore, HMF can be esterified and reduced to 2,5-bis (hydroxymethyl) furan (BHMF)[14, 15] and 2,5-dimethylfuran (DMF)[16, 17]. It can also be aminated and subjected to other catalytic reactions to yield a variety of high-value-added chemicals presenting considerable application potentials in the fields of biofuels, pharmaceuticals, polyester industry, and functional materials.[9, 18-21]

Initially, homogeneous catalysts were utilised for the catalytic oxidation of 5-HMF owing to their high activity and mild reaction conditions. [22, 23] Subsequently, non-homogeneous catalysts have been increasingly used in the 5-HMF catalytic oxidation process due to their high stability and strong catalytic activity, which includes the study of noble metal catalysts such as Ru, Pt, and Pd, as well as transition metals such as Co, Mn, Cu, and Fe.

The successful conversion of HMF to high-value-added chemicals depends largely on the reaction conditions (e.g., temperature, time, and solvent) and significantly on the characteristics of the catalysts. Compared with noble metals, transition metal catalysts have certain limitations;

however, various studies carried out so far provide promising application prospects in the preparation of HMF downstream products using transition metal catalysts. Until now, researchers have not only systematically explored the transition metal active components, reaction mechanisms, etc., but also utilized the advanced material structures, such as metal-organic framework materials (MOFs), [24, 25] hydrotalcite-like loaded catalytic materials, and non-metallic carbon-nitrogen-based catalysts, to develop effective transition metal catalysts. Moreover, single-atom catalysts have also been widely used in the catalytic reactions of HMF owing to their excellent catalytic properties.

The metal-free materials, such as carbon-based catalysts are widely used in the fields of electrochemistry, organic synthesis, and oxidation reactions due to their advantageous properties such as low cost, non-toxicity, high specific surface area, easily adjustable pore size distribution and pore structure, good electrical conductivity, and versatile chemical properties.[26-29] Recent studies have shown that the alternation in the electronic structure, surface properties, and catalytic mechanism of carbon materials mediated by doping heteroatoms such as nitrogen, phosphorus, and sulphur is an effective strategy for the development of efficient carbon catalysts.[30-32] So far, the most studied catalysts are those used for oxidation reactions, and the most studied process is the introduction of nitrogen atoms into carbon materials. A large number of active sites, high reactivity, and large specific surface area make nitrogen-doped carbon materials an efficient metal-free catalyst.

2. Application of Co-based catalysts in selective catalytic conversion of HMF

Co-based catalysts such as cobalt oxides, modified-cobalt oxides[33, 34], Co single-atom catalysts[35], Co/MOFs, and Co/C–N catalysts[36, 37] are widely used in the selective conversion of HMF.

2.1 CoO_x nanoparticles

Recently, CoO_x nanoparticles and Co single-atom catalysts were identified to exhibit catalytic conversion activity of HMF. Additionally, the catalytic performance can be improved by doping different oxides into CoO_x (Table 1). The doping of Fe_3O_4 as an acidic site provider could improve the catalytic stability. Wang.S et al. reported a new method to oxidize HMF into FDCA using magnetic nano-Fe_3O_4-CoO_x catalysts.[38] The conversion rate of HMF was 97.2%, whereas the yield of FDCA was 68.6% after 12 h of reaction at 80 ℃. Further,"the catalytic activity remained unchanged during recycling.[33] Another study showed that the formation of the predominant phase, $CoMnO_3$, in the $Mn_{0.5}O$–$Co_{0.5}O$–O and spinel $CoMn_2O_4$ hollow sphere catalysts promoted the

lattice migration of lattice oxygen O_L and also enriched the O_L content, thereby improving the catalytic activity of O_L (Fig. 2).[39, 40] Interestingly, Xu et al. prepared Co–Mn oxides (Co–Mn-0.25, 120 °C, 1 MPa O_2, 5 h) using the solid-state milling method and achieved the FDCA yield of 95%, which is superior to pure MnO_x (Fig. 3).[41] The excellent catalytic performance of the Co–Mn-0.25 catalyst is attributed to its high O_L mobility and variable oxidation state of Mn. Recently, Lin et al. [42] further investigated the effect of oxygen vacancy, O_v, and concentration of Mn–Co oxides on their catalytic performance for the oxidation of HMF. The experimental results and theoretical calculations demonstrated that increasing the amount of O_v improved the O_L reactivity of Mn–Co oxides by weakening the Mn–O bond strength. Additionally, such an increase promoted the adsorption and activation of HMF and O_2 on the catalysts (Fig. 4). In addition, uniformly distributed 25 nm CoO_x nanoparticles (NPs) on mesoporous carbon (MC) were prepared using the ion exchange and calcination method. The 2,5-furandicarboxylic acid (FDCA) yield using the above compound after 30 h was up to 95% at 80 °C under an O_2 atmosphere of 5 bar pressure.[43] The mesoporous carbon not only facilitates the dispersion of the active substances but also adsorbs OH, thereby promoting the hydrolysis of 5-HMF and the desorption of the intermediate product 5-hydroxymethyl-2-furancarboxylic acid (HMFCA). High Dimethylfuran-2,5-dicarboxylate (FDCAM) yield and selectivity were obtained by using the carbon material loaded cobalt oxide catalyst(Co_xO_y-N@C) catalyst with O_2 as the oxidant. The yield was unaffected even after recycling the Co_xO_y-N@C catalyst for five cycles.[44] Salazar et al reported the selective oxidative esterification of HMF using Co_xO_y-N@C catalyst with oxygen (from the air) as the oxidizing agent under mild conditions. A synergistic effect was observed between the cobalt oxide and nitrogen-doped carbon. Kinetic analysis showed that the cobalt catalyst had a first-order dependence on the substrate. Oxygen diffusion was demonstrated to be the limiting factor in the system.[45] Cobalt oxide not only oxidizes HMF efficiently under alkaline conditions but also maintains excellent activity under liquid-free alkaline conditions. The results are listed in Table 1.

In addition to cobalt oxide, Co single-atom catalysts and Co^{2+} complexes also exhibit excellent catalytic activity. Liu et al. prepared atomically dispersed single-atom cobalt over nitrogen-doped carbon catalysts using Co and Zn MOF decomposition strategy(Co SAs/N @ C).[46] As the monoatomic catalysts have the highest atom utilization rate, the Co monoatomic catalysts exhibited an accelerated reaction rate and 99% FDCA yield after 3 h. In addition, Jin et al. examined Ce oxide-based catalysts with different Co/Ce molar ratios (denoted as CoCe-x, with x denoting the Co/Ce

ratio) as catalysts for the oxidation of 5-HMF to 2,5- FDCA. The cobalt–cerium ratio, catalyst dosage, and reaction temperature had a significant effect on the yield and selectivity.[47] After 4 h, the complete conversion of 5-HMF with 86.3% FDCA selectivity was achieved upon using CoCe-0.15 catalyst at 130 °C under 0.6 MPa of O_2 pressure. The effective reactivity was attributed to the high specific surface area and high oxygen vacancy concentration of the catalyst that facilitated the migration and adsorption of oxygen species. In addition, the CoCe-0.15 catalyst was recycled five times without significant activity loss. Compared with cobalt oxide and Co monoatom, Co(II) -meso-tetrakis (4-pyridyl)-porphyrin (M -resin-Co- Py) has negligible ability to oxidize HMF under an O_2 atmosphere. However, in the presence of tert-butyl hydroperoxide (t-BuOOH), 96% HMF conversion and 90% FDCA yield could be achieved (Fig. 5).[48] Li et al. encapsulated ultrafine metal oxide NPs into mesoporous KIT-6 (Co@KIT-6). With water as the solvent at atmospheric conditions, Co@KIT-6 showed a high FDCA yield of 99% in 2 h, and the catalyst activity was unaffected after 6 cycles. Notably, the catalytic performance of Co@KIT-6 was superior to that of most noble metal catalysts, which might be attributed to the nano-restrictive effect of the KIT-6 mesopores that prevented the aggregation and leaching of ultrafine Co_3O_4 NPs during the reaction (Fig. 6).[49]

In recent years, single-atom catalysts have garnered significant attention. Co-based catalysts have shown better catalytic activity and are used in various fields including the field of catalytic conversion of HMF.

2.2 **Co-based loaded MOF**

MOF materials have considerable application potential in the field of catalysis. These materials can be divided into three categories based on the form and type of the coordinating metal. The first category is unmodified MOF materials, i.e., MOF materials prepared by utilizing their existing functional groups or unsaturated metal coordination junctions. The second category is the MOFs encapsulated with nanoscale metal atoms inside the cavities of their regular macroporous structure. Some of the most common MOFs in this category are Pd@MOFs, Pt@MOFs, Au@MOFs, and Ni@MOFs. The third category of MOFs is similar to the second category of MOFs, except that the MOFs are encapsulated with nanoscale metal oxide atoms instead of metal atoms. Some common MOFs in this category are Fe_3O_4@MOFs and ZnO@MOFs.[50-54] The mechanism of HMF oxidation catalysed by Co-MOF is described in detail here.

MOF-derived composites can improve gas adsorption, separation, storage capacity, and

catalytic performance. They also utilize the synergistic characteristics of the two components of the composite materials to generate new applications. MOFs and their derivatives have been widely used in the fields of catalysis, hydrogen storage, and drug delivery.[55-59] Recently, researchers have been actively exploring various MOF-based catalysts to optimize the biomass conversion process. [60-62] Fang et al. sintered a MOF to form a carbon material with a specific structure and loaded it with a composite oxide of Co and Fe to catalyse the oxidation of 5-HMF to generate 2,5-diformylfuran(DFF).[63] The reaction was carried out at 100 °C under 1 MPa oxygen pressure for 6 h with the addition of Na_2CO_3 coagulant and attained a DFF yield of more than 90%. In addition, the addition of non-metallic elements also contributes, such as the addition of S avoided the aggregation of Fe ions. In addition, S doping increased the exposure of (1 1 1) crystal faces on Fe_2O_3, which in turn favored the selective oxidation reaction of HMF.[64] A novel core-shell MOF structure with a core of Co_3O_4 and Co-BTC on its outer layer was synthesised by a simple replacement of the cobalt nitrate precursor with Co_3O_4. The core-shell catalyst afforded the specific density of the acid and base site combined with the high accessibility of the HMF molecules to the active Co sites. After 1 h, the HMFCA selectivity and HMF conversion at 60 ℃ were 89% and 79%, respectively, with *t*-BuOOH as oxidant and acetonitrile as solvent.[65]

For the catalytic conversion of HMF, the Co and MOF structures played a synergistic role in the reaction process, i.e., the metal-cobalt sites on the MOFs and the metal-cobalt atoms formed a Co^{3+}/Co^{2+} redox pair and react at the same time, which enhanced the catalytic performance of the Co-based loaded MOF materials.

2.3 **Co-based loaded non-metallic (carbon-nitrogen-based) catalysts**

There are a few reports on the selective catalytic conversion of 5-HMF using nitrogen-doped carbon catalysts for the preparation of its downstream products (Table 2). Several researchers developed a nitrogen-doped activated carbon material by treating activated carbon with H_2O_2 and NH_3 and achieved DFF selectivity of 93% after 15 h at 80 °C; however, the conversion rate of 5-HMF (23%) was low.[66] Ren et al. investigated the catalytic performance of nitrogen-doped carbon materials made from pyrolyzed chitosan and urea. The DFF yield was 95.1% at 100°C under 1.0 MPa of O_2.[67] Lv et al synthesised nitrogen-doped graphene materials using high-temperature ammonia treatment and achieved complete conversion of HMF and approximately 100% DFF selectivity using 2,2,6,6-tetramethylpiperidinium oxide (TEMPO) as a co-catalyst. The drawback

of this method was the complexity of the catalyst preparation process and the failure to recycle TEMPO.[68] Further, Teng synthesised nitrogen-doped carbon materials from chitosan and achieved 95.3% of HMF conversion rate and 94.6% DFF selectivity,; however, the reaction conditions were harsh.[69]

The studies on CeO_2 (x%Bi–CeO_2/N-PCT)[70] and Co/N–C[71] showed that the nitrogen-doped carbon substrate improved the catalytic activity by providing good electron mobility and more oxygen vacancies.

Xie et al[72] developed a facile strategy for the synthesis of N-doped carbon-supported Co/Fe bimetallic catalysts (CoFe-NC) attaining an FDMC yield of 93% in an intermittent reactor. Interestingly, CoFe-NC also produced a high FDMC yield of 91% under continuous flow conditions for 80 hours (5 bar O_2, 80 ℃, and no base). Notably, this is the first time such a high FDMC yield was achieved using a non-precious metal catalyst under continuous flow conditions. The introduction of iron greatly enhanced the ionic strength of the Co-Nx species and the basicity of the catalysts, thereby improving the O_2 activation capacity and dehydrogenation activity of CoFe-NC during the oxidative esterification of HMF. This work elucidates an effective strategy for the construction of N-doped carbon-supported non-precious metal catalysts (Fig. 7).

Yu et al[73] used metallic cobalt loaded on nitrogen-doped carbon material as an effective catalyst in the reaction of FDMC preparation by oxidative esterification of HMF. The carbonization temperature had a significant effect on the morphology and structure of Co/N–C samples. Co/N–C calcination at 900 °C yielded the best catalytic performance. After 20 h, an FDMC yield of 73.8% and an HMF conversion of 91.7% were achieved using K_2CO_3 at 130 °C and under 1 MPa O_2 atmosphere (Fig. 8). In addition, a previous study[74]employed a simple method to prepare cobalt nanoparticles embedded in graphite nitrogen-rich carbon nanotubes (Co/GCN). The Co/GCN catalysts carbonized at 800 °C exhibited the best catalytic performance with 95.8% FDMC yield and 98.6% HMF conversion under moderate reaction conditions (Fig. 9).

Among the various types of loaded catalyst carriers, carbon materials are widely used in catalytic reactions owing to their controllable morphology and good chemical reactivity. Carbon carrier materials can be doped with atoms (e.g., B[75], P[76], S[77], and N[76] elements) to influence the distribution of metal nanoparticles on the carrier and change the valence state of the elements which improves their catalytic activity.[78-81] The active centres of Co-based loaded non-metallic carbon–nitrogen–based catalysts and the conversion mechanism of HMF are described here.

Owing to the difference in electronegativity between N and C atoms, upon doping N atoms into the C–C bond in carbon nanotubes, the charge is redistributed between N and C. The N–N bond is then polarized, resulting in a partial negative charge for N atoms and a partial positive charge for C atoms close to N atoms. The polarized C–N bond will lead to a partial negative charge in N atoms, whereas the C atoms close to the N atoms will have a partial positive charge. Further, the positively charged C on the GCN carbon nanotubes is conducive to the adsorption of oxygen molecules, and the reduction of the dissociation energy of O_2 occurs through electron transfer. Therefore, the introduction of N improves the electron transfer ability of Co/GCN and enhances the surface reactivity of the catalysts.[82-84]

Carbon nanotubes enhance the catalytic reaction with capped Co nanoparticles by synergistic interactions. According to previous studies, N-doped carbon nanotubes have a high flat band voltage and will accept charges from adjacent Co nanoparticles until the Fermi energy levels of the two atoms reach equilibrium, resulting in a charge transfer between Co nanoparticles and N. On the other hand, a polarisation potential is formed between the oppositely charged nitrogen-containing carbon nanotubes and Co nanoparticles to attract the oxygen molecules. It accelerates the elimination of Co–H species generated by β-H elimination during the catalytic conversion process of HMF and advances the reaction.

Therefore, the synergistic interaction between Co nanoparticles and carbon nanotubes not only ensured the smooth catalytic conversion of HMF but also caused the existence of positively charged sites in the catalyst due to the polarization after N doping. Thus, the material acts as an alkaline catalyst. The results of CO_2-TPD(temperature-programmed desorption of CO_2) characterization also indicate that the catalyst has strong basic sites.[85-87]

Based on the characteristics of the products generated and previous studies, a reaction pathway for the catalytic conversion of HMF by Co/GCN catalysis is given in Fig.8. Initially, Co acts as an electron donor, carbon nanotubes act as electron acceptors with abundant electrons on their surface, and oxygen molecules accept the abundant electrons on carbon nanotubes to form $-O^{2-}$ ions. Moreover, the aldehyde group on the HMF forms hemiacetal intermediates with the methanol solvent through a nucleophilic addition process. Superoxide radicals attack the hydroxyl group on the $-O^{2-}$ hemiacetal to form an ester group, which is then converted to -hydroxymethyl-2-methyl-furoate (HMMF) Thereafter, the hydroxyl group on the HMMF forms 5-formyl-2-methyl-furoate (FMF) by the elimination of β-H under the action of the superoxide radicals, $-O^{2-}$.The content of

HMMF shows an increasing trend and then eventually decreases, indicating that the oxidation process of the hydroxyl group on the HMF is slower. The slower reaction, oxidation of the hydroxyl group, is the rate-controlling step of the whole reaction.[88] Further, the aldehyde group on FMF also undergoes the intermediate process of hemiacetal and finally generates the downstream products in the presence of superoxide radicals.

For the catalytic conversion of HMF, Co-based and non-carbon and nitrogen materials play a synergistic role in the reaction process. While Co-based catalysts have high activity in the catalytic conversion of HMF, their stability needs to be improved. The catalytic performance of the Co-based loaded non-metallic carbon and nitrogen materials can be improved significantly by avoiding the aggregation of active-site metals. Therefore, it is necessary to establish a simple and environmentally friendly metal-free multiphase reaction system that can be operated under non-harsh conditions and ensures efficiency and stability.

3. Mn-based catalytic system

The abundant availability and excellent oxidation performance make the Mn-based catalysts an attractive choice for application in catalytic oxidation. The crystalline structure and the different oxidation states of manganese oxides increase the number of active sites, enhance the transfer of oxygen in the catalytic conversion of HMF, and promote the catalytic reaction. Based on these characteristics, the binary or ternary structures of manganese radicals are formed by adding different metallic or non-metallic elements to strengthen the interactions between active species, regulate the surface properties, and generate new active centres, thereby achieving a multi-metallic synergistic catalytic system.

3.1 **Mn-based single metal oxide catalytic system**

Hayashi et al.[89] reported oxidation of MnO_2 with $NaHCO_3$ under the conditions of 10 bar O_2, 120 °C, and a 24-hour reaction time, achieving a 95% yield of FDCA (Table 3). Further, the MnO_2-$NaHCO_3$ catalytic system was able to convert furfural and furfuryl alcohol to furfural carboxylic acid with yields of 99% and 95%, respectively. After three cycles of conversion reaction, no significant loss in catalytic activity was observed. The structure–activity relationship of six MnO_2 crystals (α-, β-, γ-, δ-, ε- and λ-MnO_2) was investigated extensively, and the results showed that the β- MnO_2, with its low vacancy formation energy and abundant planar oxygen sites, is favourable for HMF oxidation, with an FDCA yield of 91%, under optimal conditions. In addition, the

conversion of FFCA to FDCA was found to be the rate-limiting step, and the catalytic performance could be improved by increasing the surface area of β- MnO_2 (Fig. 10).[90]

Similarly, in a study on manganese-based inhomogeneous oxidation with O_2 as the sole oxidant, Hara's group [91]observed that activated MnO_2 catalysed the oxidation of HMF to FDCA more efficiently than $SrMnO_3$ in the presence of $NaHCO_3$ as an additive, achieving a yield of 91%. The mechanism followed the oxygen supplied by the catalyst itself (Mars–van Krevelen mechanism). In this process, the formation of partially reduced $MnO_{2-\delta}$ or irreversible MnOOH affected the stability of MnO_2. Therefore, crystallization is beneficial to improve the structural stability of MnO_2. It is well known that MnO_2 exhibits different crystal structures. A recent study demonstrated, through a combination of computational and experimental studies, that MnO_2 plays a crucial role in catalysing the oxidation of HMF to produce FDCA. Density functional theory (DFT) simulations showed that the vacancy formation energies of bent oxygen sites in β- and λ-MnO_2 are lower than those of planar oxygen sites in α- and γ-MnO_2, suggesting that the β- and λ-MnO_2 may be more favourable for the target reaction. Experimental studies, including kinetic, mechanistic, and spectroscopic studies, further demonstrated that the rate-determining step (generation of FDCA from FFCA) decreases the reaction rate in the order of β-MnO_2 > λ-MnO_2 > γ-MnO_2 ≈ α-MnO_2 > δ-MnO_2 > ε-MnO_2. Thus, Hara's team confirmed that a combined theoretical and experimental approach can offer a rational approach for designing efficient manganese dioxide catalysts.

Yu et al[92] oxidized HMF to DFF by molecular oxygen selective oxidation using an α-MnO_2 catalyst, and the α-MnO_2 catalyst exhibited outstanding performance compared to the other catalysts. Additionally, the solvent, isopropanol, had a significant effect on the selectivity of DFF. The selectivity of DFF was 84.3% in a continuous reaction of 4 h at 140 °C. In addition, the α-MnO_2 catalyst maintained good reusability over five cycles of reaction. The reaction pathway indicated that lattice oxygen species in α-MnO_2 were involved in the selective oxidation of hydroxyl groups in the HMF molecule (Fig. 11).

In addition to the crystal structure and different oxidation states, forming redox pairs, such as Mn^{2+}/Mn^{3+} and Mn^{3+}/Mn^{4+} also offer excellent catalytic properties to manganese oxides. Hu [93]et al. combined the redox cycling of Mn cations with abundant surface pores to prepare porous two-dimensional Mn_2O_3 nanosheets using controlled thermal treatment of Mn-based metal-organic skeleton (Mn-MOF). The prepared nanosheets (M400) exhibited excellent catalytic activity for the aerobic oxidation of HMF to FDCA. The nanosheets (M400) were subsequently calcined at 400 °C,

achieving a high FDCA yield of more than 99.5% at full conversion. This performance was significantly better than commercial Mn_2O_3 and activated MnO_2 in terms of the reaction rate. Chen et al [94]efficiently converted HMF to DFF in toluene solvent using MnO_x/HAP catalysts under alkali-free conditions. The MnOx/HAP-10.0-400 catalyst demonstrated an HMF conversion and DFF selectivity of 86.4% and 90.9%, respectively after 12 h, at 120°C under a 1.0 MPa O_2 atmosphere. Oxidation of Mn^{4+}/Mn^{3+} reduction promoted the oxidation of 5-HMF to DFF by lattice oxygen and supplemented the lattice oxygen by adsorption of O_2 molecules. Upon evaluating the recyclability, it was evident that the catalyst did not undergo a significant loss of activity for up to four cycles. Furthermore, according to the Mars–Van Krevelen mechanism, the oxidation reaction of manganese oxides closely relies on the mobility of oxygen from the external O_2 to the oxygen of the oxide lattice to complete the catalytic cycle, thereby enabling the catalyst surface regeneration. Hu et al.[93] constructed porous two-dimensional Mn_2O_3 nanoflakes (Mn_2O_3 NF) using high-temperature heat treatment of Mn-based metal-organic skeleton (MOF, Mn-TPA, TPA:terephthalic acid). The developed Mn_2O_3 catalysts had good catalytic properties, and the HMF was almost completely converted into FDCA after 24 h. No significant loss in the catalytic activity was observed after 5 cycles of reaction. Although the yield of Mn_2O_3-catalyzed FDCA was high, the low productivity severely limited its industrialization.

The strength of Mn–O in the molecular structure of monometallic oxides tends to be different from that of other compounds and can activate reactants by electron transfer. As the d electron layer of Mn^{2+} ion can easily lose or gain electrons, it has strong redox properties. Therefore, manganese-based metal oxides are widely used as catalysts for various oxidation reactions.

3.2 **Mn-based binary or ternary composite metal catalytic systems**

Mn-based composites with excellent oxygen mobility and multiple oxidation states have also shown impressive performance in the catalytic conversion of HMF in binary or ternary composite metal systems with metals (Co, Fe, Cu, etc.) and non-metals (Br, etc.) (Table 4).

MnO_x–CeO_2 [95]: Compared to single MnO_2 catalysts, Ce^{3+} and Mn^{4+} exhibited synergistic effects with Mn^{4+} ions as active sites, and the lattice oxygen transfer from CeO_2 to MnO_x enhanced the catalytic performance under moderate conditions. Under optimal conditions, the FDCA yield of MnO_x–CeO_2 (Mn/Ce = 6) was up to 91%, and the catalyst could be recycled up to five times without any loss in activity (Fig. 12). Neatu et al. reported the $Mn_{0.75}/Fe_{0.25}$ composite as a catalyst for the one-pot oxidation of HMF to FDCA. The FDCA yield was only 90%, and the main intermediate of

this reaction was FFCA. [96] Furthermore, in the absence of a catalyst, an 87% yield of FFCA was obtained in 30 min under an 8 bar O_2 atmosphere. In the reaction condition, FFCA was acidified, filtered, and then oxidized with $Mn_{0.75}Fe_{0.25}$ as the catalyst, achieving an FDCA yield of approximately 90%. In addition, $MnFe_2O_4$ resulted in an FDCA yield of 85% under alkali-free conditions with tert-butyl hydroperoxide (TBHP) as the oxidizing agent.[97] The excellent performance was attributed to the various oxidation states of Mn and the synergistic effect between Mn and Fe_2O_4. Other manganese-based bimetallic materials, such as Fe_3O_4/ Mn_3O_4, $Mn_{0.7}Cu_{0.05}Al_{0.25}$, and octahedral MnO_2 molecular sieves, also showed good selectivity for DFF.[98-10] These studies suggest that Mn can be utilized for the oxidation of HMF owing to its active site or carrier. However, further research on the catalyst material is needed to explore its application as an effective catalyst for the oxidation of HMF.

Excellent oxygen mobility and multiple oxidation states are established factors for the superior performance of various Mn-based composites, such as Co-Mn-0.2[41], $MnCo_2O_4$[101], and Mn-Fe mixed oxides.[96] Yu et al.[102]further suggested that the active M^{3+} O(-Mn)$_{4+2}$ clusters in doped (Fe, Co, and Ni) MnO_x catalysts are the main active sites for aerobic oxidation of HMF (Fig. 13). In this study a general mechanism for electron transfer within the catalytic active site for binary[103] and ternary metal oxides is also discussed in detail.[104]

Further, due to the different chemical states and specific oxidation properties, manganese-containing catalysts showed remarkable catalytic performance for the oxidation of HMF even in the absence of alkaline additives. Kim et al.[105] developed a new class of Mn–Co–O spinel-loaded Ru catalysts which resulted in remarkable FDCA yield (99.1%) and good recoverability in pure aqueous solvents. The authors attributed the excellent performance of the catalyst to the coexistence of Lewis and Brønsted acidic sites. Indeed, this solid carrier can be regarded as a heterogeneous replica of homogeneous Co $(OAc)_2$/$Mn(OAc)_2$/HBr oxidation of HMF, which may have undergone a similar redox cascade.[106] Gao et al.[107] used Mn–Ce mixed-oxide-loaded Ru NPs ($Ru/Mn_XCe_1O_Y$) as a base-free catalyst for HMF oxidation to generate the final product FDCA after a reaction pathway with DFF as an intermediate product. The strong metal-carrier interactions and synergism between Ce and Mn oxides were prominent reasons for the superior performance of $Ru/Mn_XCe_1O_Y$. The high catalytic activity resulted in an FDCA yield of 95% (TOF $^{-5.3}$ h^{-1}), and the catalytic activity was unaffected for up to eight cycles of reaction. Ventura et al[108]considered the strong redox properties between MnO_2 and CuO and prepared CuO/MnO_2 catalysts for the conversion of HMF to FDCA in

the aqueous phase using O_2 as oxidant, achieving an FDCA yield of up to 98.7%. Calcination at 550 °C not only excludes carbon deposition but also restores catalytic activity by repairing the transient deactivation caused by the reduction of Cu^{2+} to Cu^0, instead of leaching. This inspired further efforts to develop suitable anti-carbon deposition catalysts. More importantly, the acid/base nature of the mixed oxides can be modulated by controlling the calcination temperature, suggesting that it is possible to regulate the distribution of the products in a pure aqueous solution.[106, 109-111]

Zhang et al.[101] synthesised a hollow hexagonal $MnCo_2O_4$ catalyst using a simple hydrothermal method and achieved a 71% FDCA yield under optimal conditions. The activity of $MnCo_2O_4$ was lower than that of most single Mn- and Co-based catalysts, and Mn^{3+} was identified as the active site using XPS analysis. Rao et al.[41] prepared a series of Co–Mn catalysts by solid-state milling. The introduction of Co only promoted the activity of MnO_x rather than directly participating in the reaction as a host element. Compared to Co–Mn catalysts prepared using the common co-precipitation method, Co–Mn-0.25 exhibited outstanding catalytic activity, yielding 95% FDCA after 5 h at 120 °C. The high activity of Co–Mn-0.25 is due to the high concentration of Mn^{3+}/Mn^{2+} redox pairs, as well as an abundance of reactive lattice oxygen. Similarly, Liu et al.[42] altered the concentration of oxygen vacancies in mesoporous Mn–Co spinel using a vitamin C (VC)-modified solid-state milling method and the synthesised $Mn_3Co_2O_{x-0.3}$ VC catalyst exhibited excellent HMF oxidation ability. DFT calculations indicated that oxygen vacancies weakened the strength of the Mn–O bond, which enhanced the adsorption of oxygen by lattice oxygen and thus improved the oxidation activity of the catalyst.

Cu and Mn composite catalysts are generally classified into two types: Cu-doped MnO_2 and Co–Mn oxide. Heteroatom doping is a common method to improve the catalyst activity. Feng et al.[112] reported Cu-doped MnO_2 nanorods (Cu-MnO_2 NR) prepared using a simple hydrothermal method. When tert-butanol was used as the solvent and TBHP was used as an oxidant, the FDCA yield reached 96% due to the synergistic interaction between Cu and Mn. Lai et al (Fig. 14).[113]reported another Cu-doped MnO_2 catalyst (Cu-MnO_2 @PDVTA), which achieved a 97% FDCA yield under similar reaction conditions. The nitrogen-containing polymer with a high specific surface area had abundant active basic sites due to the Cu^{2+} doping, which promoted the exchange of Mn^{4+} and Mn^{3+} as well as the mobilization of lattice oxygen. The synergistic effect of Cu^{2+}, Mn^{4+}, and Mn^{3+} with nitrogen-containing polymer bases significantly improved the reaction efficiency.

In addition to Cu-doped MnO_2, various Mn–Cu oxides have also been used to oxidize HMF.

Wang et al.[114] synthesised $CuMn_2O_4$ using a simple co-precipitation method with t-BuOOH as the oxidant, which resulted in high catalytic activity. The generation of Cu^{2+}/Cu^{+} redox pairs facilitated the conversion of Mn^{3+} to Mn^{4+}, which accelerated the reaction rate and yielded a 96% FDCA yield after 12 h at 80 °C. However, when O_2 was used as the oxidant, the activity of Mn–Cu oxides was not as prominent as that of binary Co–Mn oxides (Fig. 15). Dong et al.[115] prepared a composite catalyst (CMO-500) of Mn_2O_3 and $Cu_{1.4}Mn_{1.6}O_4$ using electrostatic spinning and heat treatment. Under optimal reaction conditions, the FDCA yield of CMO-500 could reach 94%. This was attributed to the fact that Cu^{+} regulated the coordination state of oxygen vacancies and promoted the activation of O_2. Wan et al.[116] reported a manganese copper oxide catalyst, $CuMn_2O_4$, which consists of an optimum ratio of lattice oxygen to adsorbed oxygen content. It facilitated oxygen transfer and consumption, thereby accelerating the oxidation reaction and providing 92% FDCA yield at 120 °C, 10 bar O_2, and 18 h. The reaction conditions of CMO-500 were also reported in this study.

Other Mn-based binary or ternary non-precious metal catalysts, such as Mn–La, have also been reported. Recently, Yu et al.[117] prepared La-doped MnO_2 using a simple hydrothermal method. The doping of La resulted in abundant oxygen vacancies and reactive oxygen species. Therefore, the valence state of Mn ions was changed, and the oxidizing ability of La-MnO_2 was improved, achieving a yield of 4.750 mmol FDCA $gcat^{-1}$ h^{-1} in volatile alkali ($NH_3 \cdot H_2O$). Moreover, the La–MnO_2 catalyst prepared by Yu et al.[117] showed excellent performance in the aerobic oxidation of HMF to FDCA. Characterization of the samples showed that the loose surface morphology and high oxygen mobility facilitated the increase in the oxidation reaction of HMF. H_2O is confirmed to be a good solvent for the formation of FDCA as it promotes the hydration of the aldehyde to obtain a carboxyl compound on the HMF molecule. Under mild conditions, 95.4% FDCA selectivity and and 96.3% HMF conversion were achieved in H_2O (Fig. 16).

Overall, the introduction of additional metal elements could enhance the interactions between active sites, change the surface properties of the catalyst, or form new active sites. Therefore, binary and ternary non-precious metal catalysts exhibit better oxidation and cyclic regeneration than single non-precious metal catalysts.

4. The oxidants

The 5-HMF oxidative conversions with different oxidants were listed in Table 5. The traditional methods for the oxidative conversion of 5-HMF use an excess of potassium

permanganate,[118] potassium dichromate, or high-valent lead compounds, etc. as oxidants, however, the method is a stoichiometric oxidation method, which consumes a large number of oxidants, has low atomic utilisation, and generates some toxic by-products.

The use of O_2 as a green oxidizer for the oxidation of HMF has gradually become one of the main ways. Nie and Liu reported the aerobic oxidation of HMF over manganese oxide and OMS-2 in DMF to DFF in the presence of molecular oxygen. OMS-2 showed impressive activity for HMF conversion (100%) and DFF yield (97%) at 110℃and 5 bar O_2. The authors proposed a two-step redox cycle between Mn^{4+} and Mn^{3+} under oxygen conditions. By consuming the readily available lattice oxygen in OMS-2, HMF oxidizes to form DFF, which reduces Mn^{4+} to Mn^{3+}; meanwhile, Mn^{3+} is re-oxidized by molecular oxygen to Mn^{4+}, completing the catalytic cycle, and molecular oxygen plays an important role in this process. [119,120] Mn_3O_4 NPs have been reported on the efficiently conversion of HMF to DFF in DMF under oxygen atmosphere, with a quantitative of 83% DFF yield. [98] In addition, Duan et al. [34] investigated the effect of oxygen donor and found that molecular oxygen was the optimal oxidizing agent over 5%Mn/CoO_x compared to t-BuOOH and H_2O_2. The solubility of O_2 in solvent is closely related to the activation of O_2, so the reaction efficiency is affected directly by the solubility of the reaction medium. The DFF yields were 82%, 80% and the HMF conversions were 96%, 100% at 120℃ for 12h under oxygen in methyl isobutyl ketone (MIBK) and 4-chlorotoluene solutions respectively. Otherwise, the DFF yield decreased to 65% after 4 h using trifluoro toluene as solvent, and other organic solvents (tetrahydrofuran, acetonitrile, dimethyl sulfoxide, dimethyl formamide and toluene) gave 6-55% DFF yields and 18-80% HMF conversions. [121]

H_2O_2, tert-butyl hydroperoxide (t-BuOOH) and NaClO are often used as oxidizing agents to directly oxidize HMF. The FDCA was the main product obtained with the H_2O_2 in a homogeneous system. it was proposed that HOO- generated form H_2O_2 under alkaline conditions is the key oxidizing species. [122,123]. Heterogenous systems are preferred for large-scale synthesis due to easy catalyst separation. To oxidize HMF by H_2O_2 over loaded ruthenium (10 wt% Ru/Ac) sample in alkaline solution, the FDCA yield was about 91% in Na_2CO_3 solution at 75℃ for 6 h, and 92% FFCA was obtained in 1 h at 75℃in $NaHCO_3$ solution. [18] H_2O_2 as an oxidizing agent can improve the oxidation of HMF to FDCA in a heterogenous system with some catalysts, such as Au/TiO_2[124], CoFe/SBA-15[125], titanium silicate-1 (TS-1) [126, 127], CuFe [128] and Co-Cu/AC [129]. A high FDCA yield was also obtained with t-BuOOH as oxidizing agent. Yang et al. [130] prepared nitrogen-doped

graphene (NG) layer-encapsulated copper nanoparticles (NPs) and achieved 95.2% FDCA yield under mild reaction conditions with t-BuOOH as oxidizing agent. The reaction pathway via HMF-DFF-FFCA-FDCA was also proposed. Alina et al. [131] investigated in multifunctional magnetic nanocomposite catalysts, a synergistic effect between MO_x and Nb species was found in the process of activating t-BuOOH. 93.5 % FDCA yield was obtained over the 10Co@22Nb@MNP sample. Subsequently, the synergistic effect of MO_x and Nb species in t -BuOOH activation and HMF oxidation was also confirmed on a MO_x @Nb/zeolite sample, the further oxidation of HMFCA to FDCA was prevented by the presence of predominantly acidic sites in this system. [132] Furthermore, Liu et al. [133] prepared an innovative NiO_x catalyst using NaClO as an oxidant to obtain high FDCA yields (97%), The catalytic system has a FDCA production rate of 404 μmol g^{-1} min^{-1} (13-67 times higher than FDCA production catalytic systems reported recently).

Most transition metal catalysts, Co and Mn-based catalysts, exhibit excellent oxidize ability when t-BuOOH or H_2O_2 are used as oxidants compared to air or O_2, and the reaction process is not polluting, but an excess of oxidizing agent is usually required, which not only increases the cost of the separation, but also increases the unnecessary safety risk of oxidant storage and self-decomposition. It is key to choose a highly active catalyst in the oxidation reactions using organic peroxides as the oxidant. Recently, with the development and application of catalysts, organic peroxide oxidation has become one of the oxidation methods with excellent application prospects.

Conclusions and outlook

The oxidation of 5-hydroxymethylfurfural (HMF) for the preparation of high-value-added intermediates such as 2,5 furandicarboxylic acid (FDCA) has been a trending research domain in recent years. These compounds have high added value, especially for certain applications such as synthetic materials, biomedical materials, and pesticides. Economically, it is crucial to reduce the dependence on mineral resources and to achieve the purpose of environmental protection. In conclusion, extensive research on HMF has been carried out in laboratories, and the studies gradually move towards product development for achieving sustainability. However, a large-scale and economical oxidative conversion process of HMF has not been accomplished so far. The development of catalysts, the optimisation of the reaction process, and the separation and purification of the products need to be studied in depth in the future.

While noble metals have demonstrated excellent catalytic activity and stability in HMF

conversion, the selection and adoption of transition metals have become a major research focus in the field of HMF catalytic conversion. Although transition metals have shown excellent catalytic activity in HMF selective oxidation, they still encounter deactivation challenges, especially the decrease in activity and selectivity owing to the structural damage of the catalysts caused by corrosion or carbon accumulation.

Transition metal-based catalysts, specifically cobalt- and manganese-based catalysts and their reactions, are summarized in this paper. With the limited progress in this area, the catalytic performance of Co nanoparticle and Co single metal catalysts surpasses that of most noble metal catalysts. The FeOx catalyst could improve the catalytic stability, whereas MnOx and CeOx doping could increase the activated O species. Notably, the catalytic performance increased significantly upon reinforcing MOFs and non-metallic C–Ns as supporters. It is also beneficial to the "dual-carbon" strategy as the source for C and N is also the biomass. The MnOx catalyst yielded 100% HMF conversion and 99% FDCA yield using either a single MnO_2 species or modified MnOx compounds.

Overall, the sustainable development strategy necessitates the exploration of new technologies for the catalytic conversion of HMF that are cost-effective, easy to operate, and efficient. This endeavour towards achieving the goal of efficient utilization of renewable energy is crucial. The constraints in today's technological advancements have hindered the progress of harnessing biomass energy, and the industrialisation of the catalytic conversion of biomass platform molecules into HMF has not yet been realised. Sustained research coupled with profound theoretical understanding is essential for making breakthroughs in biomass conversion in the future. With the promotion of the "dual-carbon" strategy worldwide, we believe that the efficient production technology and environmentally friendly production process of high-value-added biomass-based chemicals by catalytic conversion of HMF will be realized.

Overall, among the various catalysts, the transition-metal and C–N catalysts have been proven to be efficient for the conversion of HMF into value-added products. Therefore, it is particularly important to develop more stable and efficient transition-metal and C–N catalysts. Further, to enhance the performance of catalysts, theoretical studies on the selection, ratio, and interaction of metal carriers and their catalytic conversion mechanisms are needed.

ACKNOWLEDGMENTS

Financial support from the Natural Science Foundation of China under Contracts (21808163) is gratefully acknowledged.

Refernces:

[1] R J. Putten, J. C. Waal, E. Jong, C. B. Rasrendra, H. J. Heeres, J. G. Vries, *Chem. Rev.* **2013,** *113, 3,* 1499-1597

[2] P. L. Arias, J. A. Cecilia, I. Gandarias, J. Iglesias, M. L. Granados, R. Mariscal, G. Morales, R. Moreno-Tost, P. Maireles-Torres, *Catal. Sci. Technol.* **2020**, *10*, 2721-2757.

[3] Y. H. Liao, B. O. de Beeck, K. Thielemans, T. Ennaert, J. Snelders, M. Dusselier, C. M. Courtin, B. F. Sels, *Mol. Catal.* **2020**, *487*, 34.

[4] S. Morales-delaRosa, J. M. Campos-Martin, J. L. G. Fierro, *Cellulose* **2014**, *21*, 2397-2407.

[5] F. Delbecq, C. Len, *Molecules* **2018**, *23*, 16.

[6] T. W. Tzeng, P. Bhaumik, P. W. Chung, *Mol. Catal.* **2019**, *479*, 164-169.

[7] J. Tacacima, S. Derenzo, J. G. R. Poco, *Mol. Catal.* **2018**, *458*, 180-188.

[8] J. J. Bozell, G. R. Petersen, *Green Chem.* **2010**, *12*, 539-554.

[9] D. Y. Zhao, T. Su, Y. T. Wang, R. S. Varma, C. Len, *Mol. Catal.* **2020**, *495*, 19.
[10] N. Jacquel, R. Saint-Loup, J. P. Pascault, A. Rousseau, F. Fenouillot, *Polymer* **2015**, *59*, 234-242.
[11] G. Z. Papageorgiou, D. G. Papageorgiou, Z. Terzopoulou, D. N. Bikiaris, *Eur. Polym. J.* **2016**, *83*, 202-229.
[12] H. M. Sun, R. H. Xu, X. Jia, Z. Y. Liu, H. J. Chen, T. L. Lu, *Biomass Convers. Biorefinery* **2023**, 18.
[13] Y. Rodenas, R. Mariscal, J. L. G. Fierro, D. M. Alonso, J. A. Dumesic, M. L. Granados, *Green Chem.* **2018**, *20*, 2845-2856.
[14] T. Pasini, G. Solinas, V. Zanotti, S. Albonetti, F. Cavani, A. Vaccari, A. Mazzanti, S. Ranieri, R. Mazzoni, *Dalton Trans.* **2014**, *43*, 10224-10234.
[15] P. Lanzafame, D. M. Temi, S. Perathoner, G. Centi, A. Macario, A. Aloise, G. Giordano, *Catal. Today* **2011**, *175*, 435-441.
[16] A. Iriondo, A. Mendiguren, M. B. Güemez, J. Requies, J. F. Cambra, *Catal. Today* **2017**, *279*, 286-295.
[17] H. Y. Wang, C. H. Zhu, D. Li, Q. Y. Liu, J. Tan, C. G. Wang, C. L. Cai, L. L. Ma, *Renew. Sust. Energ. Rev.* **2019**, *103*, 227-247.
[18] C. T. Chen, C. V. Nguyen, Z. Y. Wang, Y. Bando, Y. Yamauchi, M. T. S. Bazziz, A. Fatehmulla, W. A. Farooq, T. Yoshikawa, T. Masuda, K. C. W. Wu, *ChemCatChem* **2018**, *10*, 361-365.
[19] X. L. Tong, Y. Ma, Y. D. Li, *Appl. Catal. A-Gen.* **2010**, *385*, 1-13.
[20] H. A. Xia, S. Q. Xu, H. Hu, J. H. An, C. Z. Li, *RSC Adv.* **2018**, *8*, 30875-30886.
[21] T. Su, D. Y. Zhao, Y. T. Wang, H. Y. Lü, R. S. Varma, C. Len, *ChemSusChem* **2021**, *14*, 266-280.
[22] B. Saha, S. Dutta, M. M. Abu-Omar, *Catal. Sci. Technol.* **2012**, *2*, 79-81.
[23] T. S. Hansen, I. Sádaba, E. J. García-Suárez, A. Riisager, *Appl. Catal. A-Gen.* **2013**, *456*, 44-50.
[24] Y. X. Feng, H. X. Guo, R. L. Smith, X. H. Qi, *J. Colloid Interface Sci.* **2023**, *632*, 87-94.
[25] L. Wang, J. L. Zuo, Q. T. Zhang, F. Peng, S. Z. Chen, Z. L. Liu, *Catal. Lett.* **2022**, *152*, 361-371.
[26] J. Niu, R. Shao, M. Y. Liu, Y. X. Zan, M. L. Dou, J. J. Liu, Z. P. Zhang, Y. Q. Huang, F. Wang, *Adv. Funct. Mater.* **2019**, *29*, 23.
[27] W. G. Chong, F. Xiao, S. S. Yao, J. Cui, Z. Sadighi, J. X. Wu, M. Ihsan-Ul-Haq, M. H. Shao, J. K. Kim, *Nanoscale* **2019**, *11*, 6334-6342.
[28] L. B. Zeng, X. Y. Li, S. Y. Fan, J. C. Mu, M. C. Qin, X. Y. Wang, G. Q. Gan, M. Tadé, S. M. Liu, *ACS Sustain. Chem. Eng.* **2019**, *7*, 5057-5064.
[29] G. Murdachaew, K. Laasonen, *J. Phys. Chem. C* **2018**, *122*, 25882-25892.
[30] M. A. Patel, F. X. Luo, K. Savaram, P. Kucheryavy, Q. Q. Xie, C. Flach, R. Mendelsohn, E. Garfunkel, J. V. Lockard, H. X. He, *Carbon* **2017**, *114*, 383-392.
[31] H. Jiang, Y. Q. Wang, J. Y. Hao, Y. S. Liu, W. Z. Li, J. Li, *Carbon* **2017**, *122*, 64-73.
[32] H. Liu, Y. Zhang, R. Y. Li, X. L. Sun, S. Desilets, H. Abou-Rachid, M. Jaidann, L. S. Lussier, *Carbon* **2010**, *48*, 1498-1507.
[33] J. Ren, K. H. Song, Z. Li, Q. Wang, J. Li, Y. X. Wang, D. B. Li, C. K. Kim, *Appl. Surf. Sci.* **2018**, *456*, 174-183.
[34] S. Biswas, B. Dutta, A. Mannodi-Kanakkithodi, R. Clarke, W. Q. Song, R. Ramprasad, S. L. Suib, *Chem. Commun.* **2017**, *53*, 11751-11754.
[35] P. P. Yang, Q. N. Xia, X. H. Liu, Y. Q. Wang, *Fuel* **2017**, *187*, 159-166.
[36] Y. C. Fen, W. L. Jia, G. H. Yan, X. H. Zeng, J. Sperry, B. B. Xu, Y. Sun, T. Z. Lei, L. Lin, *J. Catal.* **2020**, *381*, 570-578.
[37] Q. Zhu, F. S. Wang, F. W. Zhang, Z. P. Dong, *Nanoscale* **2019**, *11*, 17736-17745.

[38] S. G. Wang, Z. H. Zhang, B. Liu, *ACS Sustain. Chem. Eng.* **2015**, *3*, 406-412.
[39] Z. Y. Gui, S. Saravanamurugan, W. R. Cao, L. Schill, L. F. Chen, Z. W. Qi, A. Riisager, *ChemistrySelect* **2017**, *2*, 6632-6639.
[40] L. Ding, W. Y. Yang, L. F. Chen, H. Y. Cheng, Z. W. Qi, *Catal. Today* **2020**, *347*, 39-47.
[41] K. T. V. Rao, J. L. Rogers, S. Souzanchi, L. Dessbesell, M. B. Ray, C. B. Xu, *ChemSusChem* **2018**, *11*, 3323-3334.
[42] H. Liu, W. L. Jia, X. Yu, X. Tang, X. H. Zeng, Y. Sun, T. Z. Lei, H. Y. Fang, T. Y. Li, L. Lin, *ACS Catal.* **2021**, *11*, 7828-7844.
[43] X. Y. Liu, M. Zhang, Z. H. Li, *ACS Sustain. Chem. Eng.* **2020**, *8*, 4801-4808.
[44] J. Deng, H. J. Song, M. S. Cui, Y. P. Du, Y. Fu, *ChemSusChem* **2014**, *7*, 3334-3340.
[45] A. Salazar, P. Hünemörder, J. Rabeah, A. Quade, R. V. Jagadeesh, E. Mejia, *ACS Sustain. Chem. Eng.* **2019**, *7*, 12061-12068.
[46] H. Zhou, H. H. Xu, X. K. Wang, Y. Liu, *Green Chem.* **2019**, *21*, 2923-2927.
[47] M. M. Jin, L. H. Yu, H. Chen, X. L. Ma, K. Cui, Z. Wen, Z. W. Ma, Y. S. Sang, M. M. Chen, Y. D. Li, *Catal. Today* **2021**, *367*, 2-8.
[48] L. C. Gao, K. J. Deng, J. D. Zheng, B. Liu, Z. H. Zhang, *Chem. Eng. J.* **2015**, *270*, 444-449.
[49] R. Q. Fang, P. L. Tian, X. F. Yang, R. Luque, Y. W. Li, *Chem. Sci.* **2018**, *9*, 1854-1859.
[50] I. Luz, C. Rösler, K. Epp, F. Xamena, R. A. Fischer, *Eur. J. Inorg. Chem.* **2015**, 3904-3912.
[51] Q. R. Fang, D. Q. Yuan, J. Sculley, J. R. Li, Z. B. Han, H. C. Zhou, *Inorg. Chem.* **2010**, *49*, 11637-11642.
[52] A. Dhakshinamoorthy, A. M. Asiri, H. Garcia, *ACS Catal.* **2017**, *7*, 2896-2919.
[53] X. F. Hu, Z. Q. Zhu, F. Y. Cheng, Z. L. Tao, J. Chen, *Nanoscale* **2015**, *7*, 11833-11840.
[54] Q. Yang, W. X. Liu, B. Q. Wang, W. N. Zhang, X. Q. Zeng, C. Zhang, Y. J. Qin, X. M. Sun, T. P. Wu, J. F. Liu, F. W. Huo, J. Lu, *Nat. Commun.* **2017**, *8*, 9.
[55] A. U. Czaja, N. Trukhan, U. Müller, *Chem. Soc. Rev.* **2009**, *38*, 1284-1293.
[56] S. Chaemchuen, N. A. Kabir, K. Zhou, F. Verpoort, *Chem. Soc. Rev.* **2013**, *42*, 9304-9332.
[57] C. Y. Sun, C. Qin, C. G. Wang, Z. M. Su, S. Wang, X. L. Wang, G. S. Yang, K. Z. Shao, Y. Q. Lan, E. B. Wang, *Adv. Mater.* **2011**, *23*, 5629-+.
[58] Y. J. Cui, B. Li, H. J. He, W. Zhou, B. L. Chen, G. D. Qian, *Accounts Chem. Res.* **2016**, *49*, 483-493.
[59] M. I. Nandasiri, S. R. Jambovane, B. P. McGrail, H. T. Schaef, S. K. Nune, *Coord. Chem. Rev.* **2016**, *311*, 38-52.
[60] M. Anbia, S. Sheykhi, *J. Nat. Gas Chem.* **2012**, *21*, 680-684.
[61] J. M. Du, H. H. Fang, H. Y. Qu, J. P. Zhang, X. P. Duan, Y. Z. Yuan, *Appl. Catal. A-Gen.* **2018**, *567*, 80-89.
[62] J. J. Zhao, Y. L. Zhang, K. Wang, C. H. Yan, Z. L. Da, C. X. Li, Y. S. Yan, *ChemistrySelect* **2018**, *3*, 11476-11485.
[63] R. Q. Fang, R. Luque, Y. W. Li, *Green Chem.* **2016**, *18*, 3152-3157.
[64] R. Q. Fang, R. Luque, Y. W. Li, *Green Chem.* **2017**, *19*, 647-655.
[65] M. Bordeiasu, A. Ejsmont, J. Goscianska, B. Cojocaru, V. I. Parvulescu, S. M. Coman, *Appl. Catal. A-Gen.* **2023**, *657*, 12.
[66] H. Watanabe, S. Asano, S. Fujita, H. Yoshida, M. Arai, *ACS Catal.* **2015**, *5*, 2886-2894.
[67] Y. S. Ren, Z. L. Yuan, K. L. Lv, J. Sun, Z. H. Zhang, Q. Chi, *Green Chem.* **2018**, *20*, 4946-4956.
[68] G. Q. Lv, H. L. Wang, Y. X. Yang, T. S. Deng, C. M. Chen, Y. L. Zhu, X. L. Hou, *ACS Catal.* **2015**, *5*, 5636-5646.

[69] N. Teng, J. L. Li, B. Q. Lu, Y. Q. Wang, S. Y. Jia, Y. X. Wang, X. L. Hou, *New Carbon Mater.* **2019**, *34*, 593-599.

[70] Y. A. Wei, C. X. Li, C. T. Zhu, Y. L. Zhang, Z. Zhu, Y. Chen, X. Li, Y. S. Yan, *J. Taiwan Inst. Chem. Eng.* **2022**, *138*, 10.

[71] R. Kumar, Z. Zhu, C. Z. Chen, W. F. Cai, J. W. C. Wong, J. Zhao, *ChemSusChem* **2022**, *15*, 10.

[72] W. Z. Xie, B. L. Chen, W. L. Jia, H. Liu, Z. Li, S. L. Yang, X. Tang, X. H. Zeng, Y. Sun, X. X. Ke, T. Y. Li, H. Y. Fang, L. Lin, *J. Energy Chem.* **2022**, *75*, 95-108.

[73] L. H. Yu, H. Chen, Y. Y. Li, Z. Wen, Y. D. Li, *Catal. Today* **2023**, *408*, 58-63.

[74] L. H. Yu, S. Kasipandi, H. Chen, Y. Y. Li, X. L. Ma, Z. Wen, Y. D. Li, *React. Chem. Eng.* **2022**, *7*, 1191-1198.

[75] Y. Q. Zhu, W. K. Hsu, M. Terrones, N. Grobert, H. Terrones, J. P. Hare, H. W. Kroto, D. R. M. Walton, *J. Mater. Chem.* **1998**, *8*, 1859-1864.

[76] Y. J. Zhang, T. Mori, J. H. Ye, M. Antonietti, *J. Am. Chem. Soc.* **2010**, *132*, 6294-+.

[77] Z. Yang, Z. Yao, G. F. Li, G. Y. Fang, H. G. Nie, Z. Liu, X. M. Zhou, X. Chen, S. M. Huang, *ACS Nano* **2012**, *6*, 205-211.

[78] R. V. Jagadeesh, K. Natte, H. Junge, M. Beller, *ACS Catal.* **2015**, *5*, 1526-1529.

[79] Y. H. Han, Z. Y. Wang, R. R. Xu, W. Zhang, W. X. Chen, L. R. Zheng, J. Zhang, J. Luo, K. L. Wu, Y. Q. Zhu, C. Chen, Q. Peng, Q. Liu, P. Hu, D. S. Wang, Y. D. Li, *Angew. Chem.-Int. Edit.* **2018**, *57*, 11262-11266.

[80] Y. T. Zhou, Q. Y. Huang, C. T. J. Low, R. I. Walton, T. McNally, C. Y. Wan, *New J. Chem.* **2019**, *43*, 5632-5641.

[81] N. Yang, L. Li, J. Li, W. Ding, Z. D. Wei, *Chem. Sci.* **2018**, *9*, 5795-5804.

[82] B. Yue, Y. W. Ma, H. S. Tao, L. S. Yu, G. Q. Jian, X. Z. Wang, X. S. Wang, Y. N. Lu, Z. Hu, *J. Mater. Chem.* **2008**, *18*, 1747-1750.

[83] Y. G. Chen, J. J. Wang, H. Liu, R. Y. Li, X. L. Sun, S. Y. Ye, S. Knights, *Electrochem. Commun.* **2009**, *11*, 2071-2076.

[84] H. Feng, J. Ma, Z. Hu, *J. Mater. Chem.* **2010**, *20*, 1702-1708.

[85] S. Maldonado, S. Morin, K. J. Stevenson, *Carbon* **2006**, *44*, 1429-1437.

[86] Q. Zhou, Y. F. Zhang, J. Y. Zhang, D. Q. Ding, *Fuel* **2018**, *229*, 135-143.

[87] C. G. Hu, L. M. Dai, *Angew. Chem.-Int. Edit.* **2016**, *55*, 11736-11758.

[88] L. Ardemani, G. Cibin, A. J. Dent, M. A. Isaacs, G. Kyriakou, A. F. Lee, C. M. A. Parlett, S. A. Parry, K. Wilson, *Chem. Sci.* **2015**, *6*, 4940-4945.

[89] E. Hayashi, T. Komanoya, K. Kamata, M. Hara, *ChemSusChem* **2017**, *10*, 654-658.

[90] E. Hayashi, Y. Yamaguchi, K. Kamata, N. Tsunoda, Y. Kumagai, F. Oba, M. Hara, *J. Am. Chem. Soc.* **2019**, *141*, 890-900.

[91] S. Kawasaki, K. Kamata, M. Hara, *ChemCatChem* **2016**, *8*, 3247-3253.

[92] L. H. Yu, H. Chen, Z. Wen, M. M. Jin, Z. W. Ma, X. L. Ma, Y. S. Sang, M. M. Chen, Y. D. Li, *Catal. Today* **2021**, *367*, 9-15.

[93] L. W. Bao, F. Z. Sun, G. Y. Zhang, T. L. Hu, *ChemSusChem* **2020**, *13*, 548-555.

[94] H. Chen, Y. Y. Li, L. H. Yu, S. Wang, X. L. Ma, C. Wang, Y. D. Li, *Catal. Lett.* **2022**, *152*, 3716-3724.

[95] X. W. Han, C. Q. Li, X. H. Liu, Q. N. Xia, Y. Q. Wang, *Green Chem.* **2017**, *19*, 996-1004.

[96] F. Neatu, R. S. Marin, M. Florea, N. Petrea, O. D. Pavel, V. I. Pârvulescu, *Appl. Catal. B-Environ.* **2016**, *180*, 751-757.

[97] A. B. Gawade, A. V. Nakhate, G. D. Yadav, *Catal. Today* **2018**, *309*, 119-125.

[98] B. Liu, Z. H. Zhang, K. L. Lv, K. J. Deng, H. M. Duan, *Appl. Catal. A-Gen.* **2014**, *472*, 64-71.
[99] F. Neatu, N. Petrea, R. Petre, V. Somoghi, M. Florea, V. I. Parvulescu, *Catal. Today* **2016**, *278*, 66-73.
[100] B. Sarmah, R. Srivastava, *Mol. Catal.* **2019**, *462*, 92-103.
[101] S. Zhang, X. Z. Sun, Z. H. Zheng, L. Zhang, *Catal. Commun.* **2018**, *113*, 19-22.
[102] K. Yu, Y. Q. Liu, D. Lei, Y. Z. Jiang, Y. B. Wang, Y. J. Feng, L. L. Lou, S. X. Liu, W. Z. Zhou, *Catal. Sci. Technol.* **2018**, *8*, 2299-2303.
[103] H. Zhou, H. H. Xu, Y. Liu, *Appl. Catal. B-Environ.* **2019**, *244*, 965-973.
[104] A. Jain, S. C. Jonnalagadda, K. V. Ramanujachary, A. Mugweru, *Catal. Commun.* **2015**, *58*, 179-182.
[105] D. K. Mishra, H. J. Lee, J. Kim, H. S. Lee, J. K. Cho, Y. W. Suh, Y. Yi, Y. J. Kim, *Green Chem.* **2017**, *19*, 1619-1623.
[106] W. Partenheimer, V. V. Grushin, *Adv. Synth. Catal.* **2001**, *343*, 102-111.
[107] T. Y. Gao, J. Chen, W. H. Fang, Q. E. Cao, W. P. Su, F. Dumeignil, *J. Catal.* **2018**, *368*, 53-68.
[108] M. Ventura, F. Nocito, E. de Giglio, S. Cometa, A. Altomare, A. Dibenedetto, *Green Chem.* **2018**, *20*, 3921-3926.
[109] M. Ventura, M. Aresta, A. Dibenedetto, *ChemSusChem* **2016**, *9*, 1096-1100.
[110] X. L. Tong, L. N. Yu, H. Chen, X. L. Zhuang, S. Y. Liao, H. G. Cui, *Catal. Commun.* **2017**, *90*, 91-94.
[111] M. Ventura, F. Lobefaro, E. de Giglio, M. Distaso, F. Nocito, A. Dibenedetto, *ChemSusChem* **2018**, *11*, 1305-1315.
[112] F. Cheng, D. W. Guo, J. H. Lai, M. H. Long, W. G. Zhao, X. X. Liu, D. L. Yin, *Front. Chem. Sci. Eng.* **2021**, *15*, 960-968.
[113] J. H. Lai, F. Cheng, S. L. Zhou, S. Wen, D. W. Guo, W. G. Zhao, X. X. Liu, D. L. Yin, *Appl. Surf. Sci.* **2021**, *565*, 9.
[114] F. Wang, J. H. Lai, Z. X. Liu, S. Wen, X. X. Liu, *Biomass Convers. Biorefinery* **2022**, 12.
[115] X. X. Dong, X. Y. Wang, H. Song, Y. Zhang, A. H. Yuan, Z. J. Guo, Q. Wang, F. Yang, *ChemSusChem* **2022**, *15*, 12.
[116] X. Y. Wan, N. N. Tang, Q. Xie, S. Y. Zhao, C. M. Zhou, Y. H. Dai, Y. H. Yang, *Catal. Sci. Technol.* **2021**, *11*, 1497-1509.
[117] L. H. Yu, H. Chen, Z. Wen, M. M. Jin, X. L. Ma, Y. Y. Li, Y. S. Sang, M. M. Chen, Y. D. Li, *Ind. Eng. Chem. Res.* **2021**, *60*, 1624-1632.
[118] T. Miura, H. Kakinuma, T. Kono, H. Matsuhisa, JP5012348-B2, 2008.
[119] J. F. Nie, H. C. Liu, *J. Catal.* **2014**, *316*, 57-66.
[120] G. D. Yadav, R. V. Sharma, *Appl. Catal. B-Environ.* **2014**, *147*, 293-301.
[121] Y. M. Wang, B. Liu, K. C. Huang, Z. H. Zhang, *Ind. Eng. Chem. Res.* **2014**, *53*, 1313-1319.
[122] S. Zhang, L. Zhang, *Pol. J. Chem. Technol.* **2017**, *19*, 11-16.
[123] S. Li, K. M. Su, Z. H. Li, B. W. Cheng, *Green Chem.* **2016**, *18*, 2122-2128.
[124] T. Ji, C. Liu, X. H. Lu, J. H. Zhu, *ACS Sustain. Chem. Eng.* **2018**, *6*, 11493-11501.
[125] D. X. Martínez-Vargas, J. R. De La Rosa, L. Sandoval-Rangel, J. L. Guzmán-Mar, M. A. Garza-Navarro, C. J. Lucio-Ortiz, D. A. De Haro-Del Río, *Appl. Catal. A-Gen.* **2017**, *547*, 132-145.
[126] N. Alonso-Fagúndez, I. Agirrezabal-Telleria, P. L. Arias, J. L. G. Fierro, R. Mariscal, M. L. Granados, *RSC Adv.* **2014**, *4*, 54960-54972.
[127] A. C. Alba-Rubio, J. L. G. Fierro, L. León-Reina, R. Mariscal, J. A. Dumesic, M. L. Granados, *Appl. Catal. B-Environ.* **2017**, *202*, 269-280.

[128] D. Gao, F. Han, G. I. N. Waterhouse, Y. Li, L. L. Zhang, *Catal. Commun.* **2023**, *173*, 106561.

[129] T. K. T. Le, S. Kongparakul, H. B. Zhang, J. G. Zhao, G. Q. Guan, N. Chanlek, T. T. V. Tran, C. Samart, *Mol. Catal.* **2023**, *539*, 113017.

[130] C. X. Yang, X. Li, Z. Z. Zhang, B. H. Lv, J. C. Li, Z. J. Liu, W. Z. Zhu, F. R. Tao, G. Q. Lv, Y. X. Yang, *J. Energy Chem.* **2020**, *50*, 96-105.

[131] A. Tirsoaga, M. El Fergani, N. Nuns, P. Simon, P. Granger, V. I. Parvulescu, S. M. Coman, *Appl. Catal. B-Environ.* **2020**, *278*, 119309.

[132] M. El Fergani, N. Candu, P. Granger, S. M. Coman, V. I. Parvulescu, *Catal. Today* **2022**, *405*, 267-276.

[133] H. Liu, W. L. Li, M. Zuo, X. Tang, X. H. Zeng, Y. Sun, T. Z. Lei, H. Y. Fang, T. Y. Li, L. Lin, *Ind. Eng. Chem. Res.* **2020**, *59*, 4895-4904.

Table1. Catalytic performance of Co-based catalysts on HMF oxidation.

Catalyst	Solvent	Reaction conditions	Conv. (%)	Yield (%)	Ref.
Fe_3O_4-CoOx	DMSO	NaOH 12h,80℃,10 barO_2	97.2	FDCA 68.6	[38]
$Mn_{0.5}O$-$Co_{0.5}O$-O	Ethanol	2 h,140℃,30 bar Air	43	DFF 42	[39]
$CoMn_2O_4$	DMF	2 h,100℃,8 bar O_2	42	DFF 42	[40]
Co-Mn-0.25	H_2O	$NaHCO_3$（2 eq） 5 h,120℃,10 bar O_2	100	FDCA 95	[41]
CoO_x-MC	H_2O	K_2CO_3（3.6 eq） 30 h,80 ℃,5 bar O_2	98	FDCA 95	[43]
Co_xO_y-N@C+K-OMS-2	MeOH	K_2CO_3（0.2 eq） 6 h,100 ℃,10 bar O_2	100	FFCA 53	[44]
Co_xO_y-N@C+Ru@C	MeOH	K_2CO_3（0.2 eq） 16 h,50 ℃,1 bar Air	100	FFCA 100	[45]
Co SAs/N@C	H_2O	Na_2CO_3（1 eq） 8 h,85 ℃,1 bar O_2	100	FDCA 99	[46]
CoCe-0.15	DMF	base-free 4h,130℃,0.6MPa O_2	100	FDCA 86.3	[47]
M-resin-Co-Py	CH_3CN	base-free 24 h,100℃,t-BuOOH	96	FDCA 90	[48]
Co@KIT-6	H_2O	base-free 2 h,80℃,1 bar air	100	FDCA 99	[49]
Co_3O_4@CoBTC	CH_3CN	1h,t-BuOOH	79	HMFCA 89	[65]

Table2. Catalytic conversion of HMF over non-metallic carbon-nitrogen based catalysts

Catalyst	Solvent	Reaction conditions	Conv. (%)	Yield (%)	Ref.
CoO_x-MC	H_2O	K_2CO_3（3.6 eq） 30 h,80 ℃,5 bar O_2	98	FDCA 95	[43]
Co_xO_y-N@C+K-OMS-2	MeOH	K_2CO_3（0.2 eq） 6 h,100 ℃,10 bar O_2	100	FFCA 53	[44]
Co_xO_y-N@C+Ru@C	MeOH	K_2CO_3（0.2 eq） 16 h,50 ℃,1 bar Air	100	FFCA 100	[45]
Co SAs/N@C	H_2O	Na_2CO_3（1 eq） 8 h,85 ℃,1 bar O_2	100	FDCA 99	[46]
NC-950	CH_3CN	HNO_3 14h,100℃,10 bar O_2	100	DFF 95.1	[67]
rGO	CH_3CN	12h,100℃	89.4	DFF 98.8	[68]
Ch-K-700	CH_3CN	7.5 h,120℃,2.0 MPa O_2	95.3	DFF 94.6	[69]
Bi-CeO2/N-PC	CH_3CN	NaOH 12h,110℃,1.0 MPa O_2	＞60	FDCA 92.8	[70]
Co/N-C	H_2O	24h,120℃	99	FDCA 68	[71]
CoFe-NC	MeOH	base-free 4h,80℃,2bar O_2	100	FDMC 93	[72]
Co/N-C	MeOH	K_2CO_3 20h,130℃,1bar O_2	91.7	FDMC 73.8	[73]
Co/GCN	MeOH	16h,130℃,1.0 MPa O_2	98.6	FDMC 95.8	[74]

Table 3. Catalytic conversion of HMF over Mn-based metal oxides

Catalyst	HMF （mM）	Solvent	Reaction conditions	Conv. (%)	Yield(%)	Ref
MnO_2		H_2O	$NaHCO_3$ (3 eq) 24h,120℃,10 bar O_2	100	FDCA 95	[89]
MnO_2		H_2O	$NaHCO_3$ (3 eq) 24h,100℃,10 bar O_2	100	FDCA 91	[89]
$SrMnO_3$	40	H_2O	$NaHCO_3$ (3 eq) 24h,100℃,1 MPa O_2	99	FDCA 58	[89]
MnO_2	40	H_2O	$NaHCO_3$ (3 eq) 24h,100℃,1 MPa O_2	99	FDCA 91	[89]
β-MnO_2-HS	40	H_2O	$NaHCO_3$ (3 eq) 24h,100℃,1 MPa O_2	99	FDCA 86	[91]
α-MnO_2		IPA	4h,140℃	93.2	DFF 78.6	[92]
activated MnO_2	40	H_2O	$NaHCO_3$ (3 eq) 24h,100℃,1 MPa O_2	99	FDCA 74	[93]
Holey 2D Mn_2O_3	50	H_2O	$NaHCO_3$ (3 eq) 24h,100℃,1.4 MPa O_2	100	FDCA 99.5	[93]
MnO_x/HAP		CH_3CN	base-free 12h,120℃,1.0MPa O_2	86.4	DFF 90.9	[94]

Table4. Catalytic conversion of HMF over Mn-based binary or ternary composite metals

Catalyst	HMF（mM）	Solvent	Reaction conditions	Conv.(%)	Yield(%)（FDCA）	Ref
MC-6		H_2O	$KHCO_3$ (4 eq) 15h,75℃,20 bar O_2	98	91	[95]
$Mn_{0.75}/Fe_{0.25}$	100	H_2O	NaOH (4 eq) 24h,90℃,0.8MPa O_2	90	90	[96]
$MnFe_2O_4$		CH_3CN	Base free 5h,100℃,TBHP	＞80	85	[97]
$Ru/MnCo_2O_4$	100	H_2O	10h,120℃,2.4MPaAir	100	99.1	[105]
$Ru/Mn_6Ce_1O_Y$	100	H_2O	15h,150℃,1.0MPa O_2	100	99.9	[107]
$Ru/Mn_6Ce_1O_Y$	100	H_2O	18h,120℃,1.0MPa O_2	100	95	[107]
$CuO-MnO_2-CeO_2$	15	H_2O	12h,130℃,0.9MPa O_2	97.4	71	[108]
Co/Mn/Zr/Br	768	HOAc	3 h,125℃,70 bar air	100	61	[106]
Co/Mn/Br	377	HOAc	0.5 h,125℃,60 bar Air	100	83	[106]
Co/Mn/Br	926	HOAc	0.5 h,150℃,8 bar Air	100	85	[106]
Co/Mn/Br	1842	HOAc	3.7 h,180℃,30 bar Air	100	97	[106]
$Li_2CoMn_3O_8$	160	HOAc	NaBr（0.03 eq） 8 h,150℃,55 bar O_2	100	80	[104]
$MnCo_2O_4$	40	H_2O	$KHCO_3$ (3 eq) 24h,100℃,1 MPa O2	99.5	70.9	[101]
Co-Mn-0.25	50	H_2O	$NaHCO_3$ (2 eq) 5h,120℃,1 MPa O_2	99	95	[41]
$Mn_3Co_2O_x$-0.3VC	83	H_2O	$NaHCO_3$（2 eq） 3 h,130℃,15 bar Air	100	96	[42]
Cu-MnO_2 NR	17	tert-butanol	base-free 12 h, 80℃, t-BuOOH	100	96	[112]
Cu-MnO_2 @PDVTA	63	tert-butanol	base-free 24 h,80℃,t-BuOOH	100	97	[113]
$CuMn_2O_4$	74	CH_3CN	base-free 12 h,80℃,t-BuOOH	100	96	[114]
CMO-500	10	H_2O	$NaHCO_3$（2 eq） 24 h,120℃,3 bar O_2	100	94	[115]

$CuMn_2O_4$	50	H_2O	$NaHCO_3$（2 eq） 18 h,120℃,10 bar O_2	100	92	[116]
La-MnO_2	40	H_2O	$NH_3·H_2O$（0.5 eq） 4 h,140℃,5 bar O_2	96	95	[117]

Table 5. Catalytic conversion of HMF under various oxidants

Catalyst	Oxidant	Reaction conditions	Conv. (%)	Product	Yield (%)	Ref.
OMS-2	O_2	110℃,5 bar O_2,1 h	100	DFF	97.2	[119]
K-OMS-2	air	165℃,15 bar air, 4 h	62.0	DFF	51.0	[120]
Mn_3O_4	O_2	120℃,20 mLmin^{-1} O_2,4 h	100	DFF	83.2	[98]
Fe_3O_4/Mn_3O_4	O_2	120℃,20 mLmin^{-1} O_2,4 h	84–99.8	DFF	51–82	[34]
Meso 5%Mn/CoO_x	air	100–130℃,4 h	70.0-80.0	DFF	70.0-77.0	[34]
$Mn_{0.7}Cu_{0.05}Al_{0.25}$ (LDH)	O_2	90℃,8 bar,24 h	90.0	DFF	78.0	[99]
$Co_{6.6}Ce_{3.3}Ru_{1.1}$	O_2	120℃,20 mLmin^{-1} O_2,12 h	100	DFF	83	[121]
HMF/KOH/H_2O_2= 1/4/8	H_2O_2	70℃,15 min	99	FDCA	55.6	[122]
Molybdenum complex $[EMIM]_4Mo_8O_{26}$	H_2O_2	Aqueous NaOH, Catalyst/HMF=1/129, 100℃,2 h	99.5	FDCA	99.5	[123]
Ru/AC	H_2O_2	HMF/catalyst = 10, 75℃,6 h	100	FDCA	92	[18]
Ru/AC	H_2O_2	HMF/catalyst = 50, 75℃, 1 h	100	FFCA	91.3	[18]
Au/TiO_2	H_2O_2	Aqueous NaOH, microwave heating, 97℃, 30 min	100	FDCA	＞99	[124]
Co(II), Fe(III), Cu(II) salen/SBA-15	H_2O_2	25℃, 100 min	99	FDCA,	5	[125]
CuFe-LDH	H_2O_2	Aqueous NaOH, 110℃, 6 h	85	FFCA	69.5	[128]
Co-Cu/AC	H_2O_2	170℃, 9 h	99	FDCA	91	[129]
Cu/NG	t-BuOOH	70℃, 24 h	100	FDCA	95.2	[130]
10Co@22Nb@MNP	t-BuOOH	100℃, 24 h	96.9	FDCA	93.5	[131]
Mn@Nb-Y30	t-BuOOH	170℃, 12 h	95	HMFCA	92	[132]
NiO_x	NaClO	25℃, 30 min	100	FDCA	97	[133]

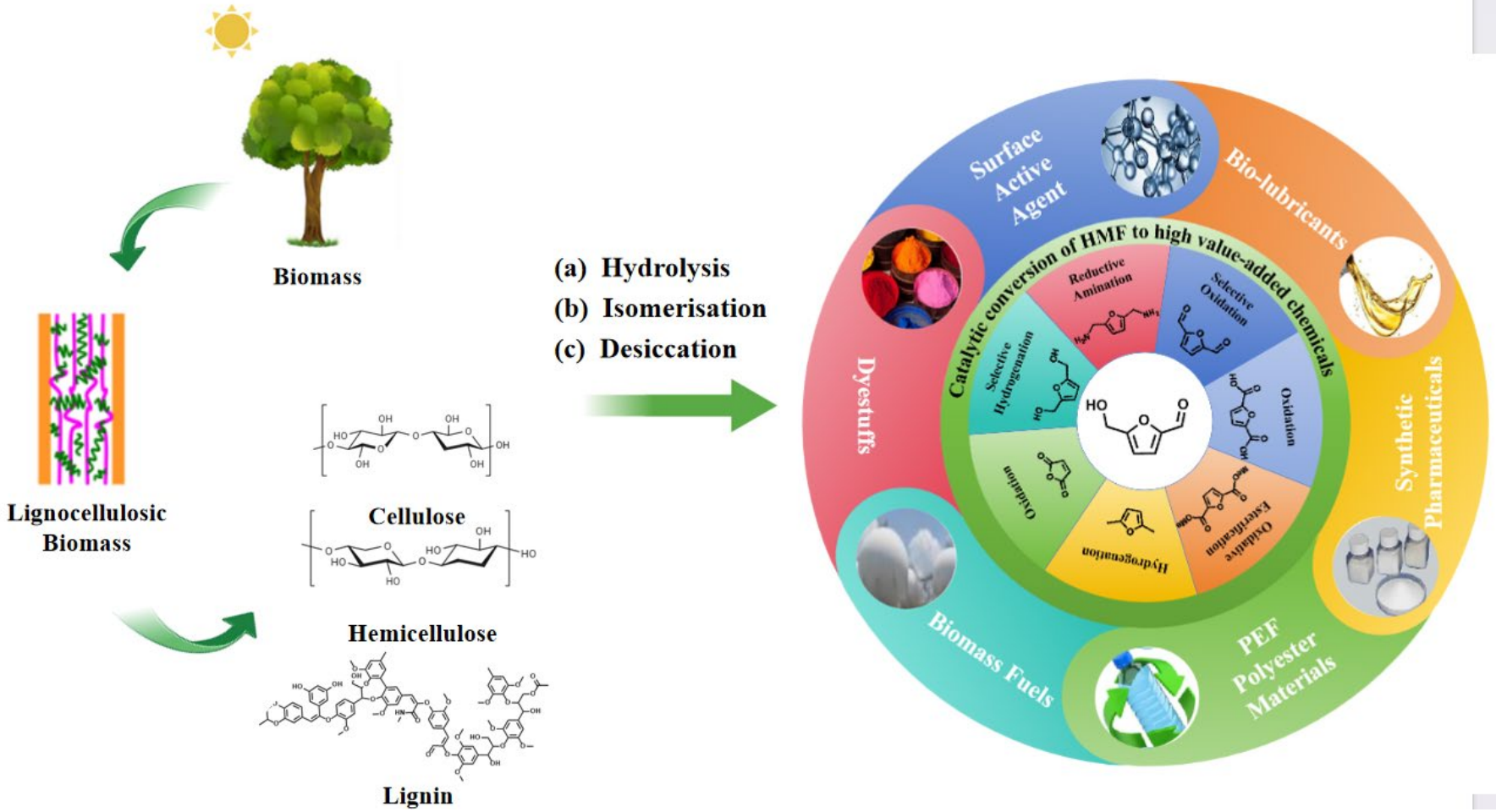

Figure 1. Catalytic conversion of HMF to high value-added chemicals

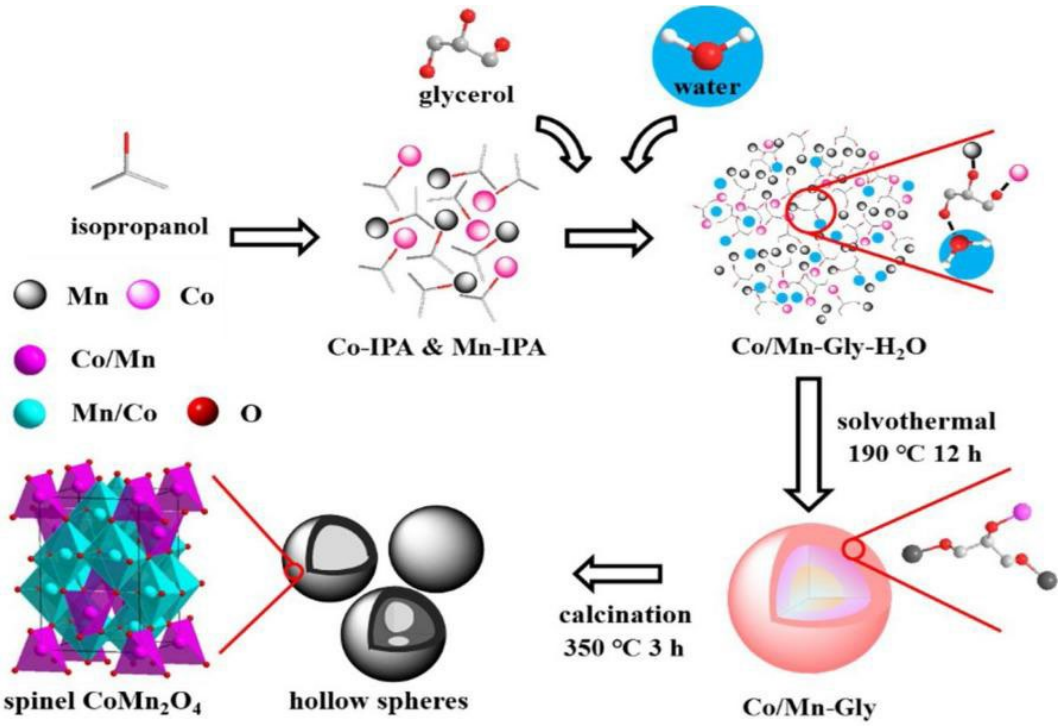

Fig 2. Schematic illustration of the formation process of spinel $CoMn_2O_4$ hollow spheres.Ref.[40].

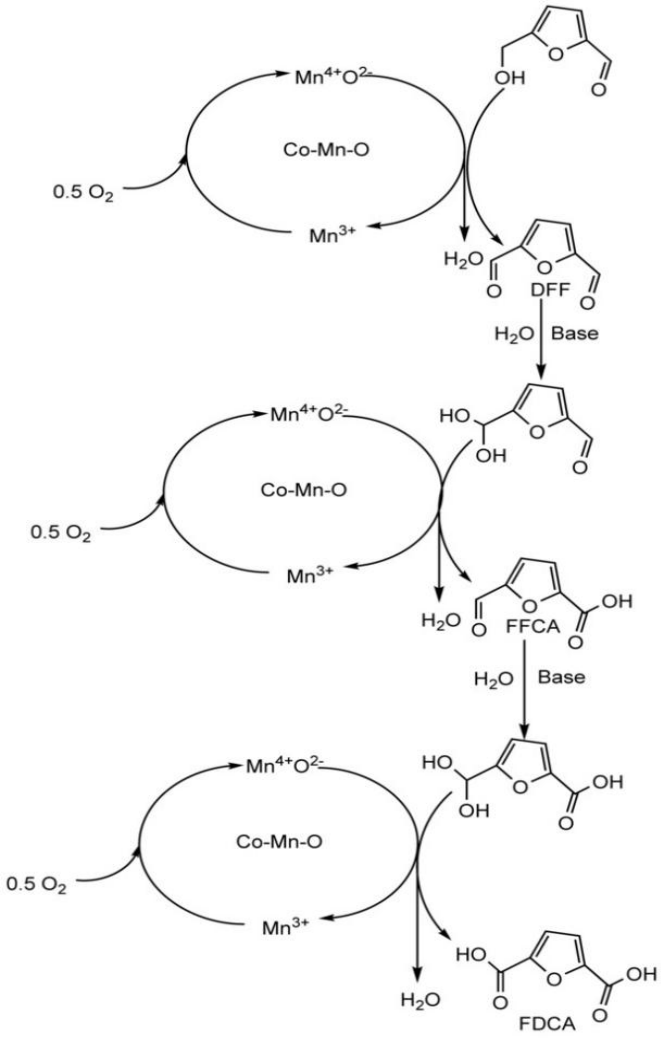

Fig 3. Plausible reaction mechanism for the selective oxidation of HMF to FDCA over Co-Mn-O catalyst.Ref.[41].

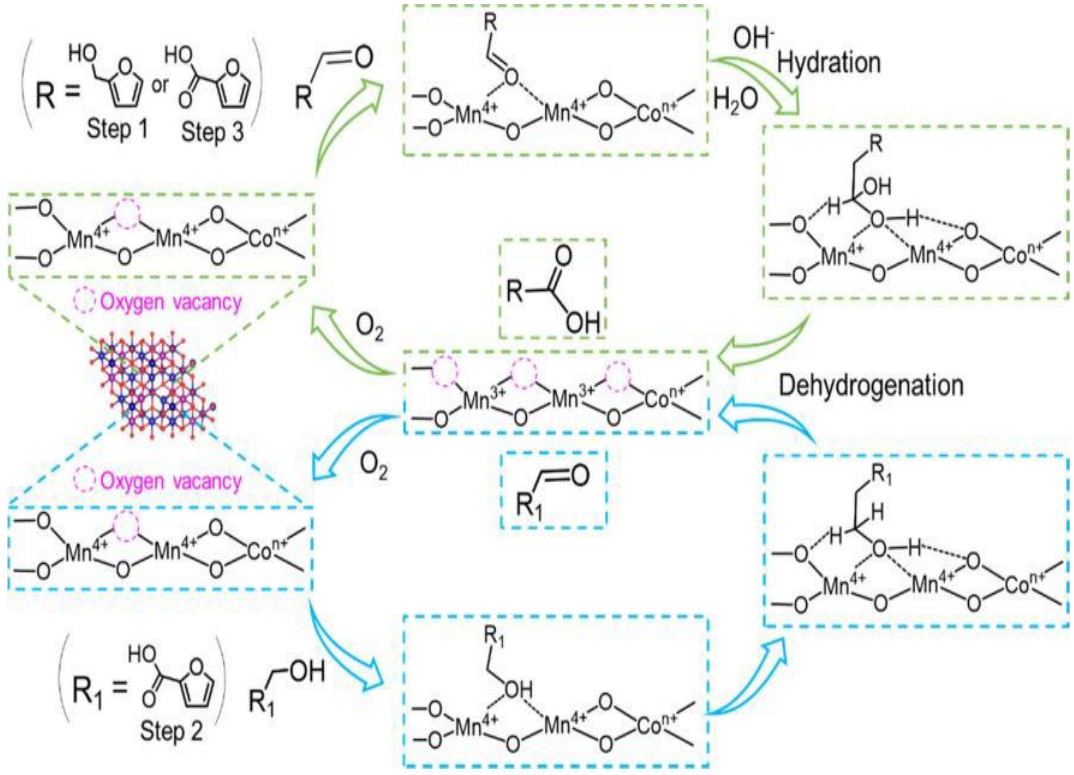

Fig 4. Probable Reaction Mechanism for the Oxidation of HMF to FDCA over $Mn_3Co_2O_x$-0.3VC.Ref. [42].

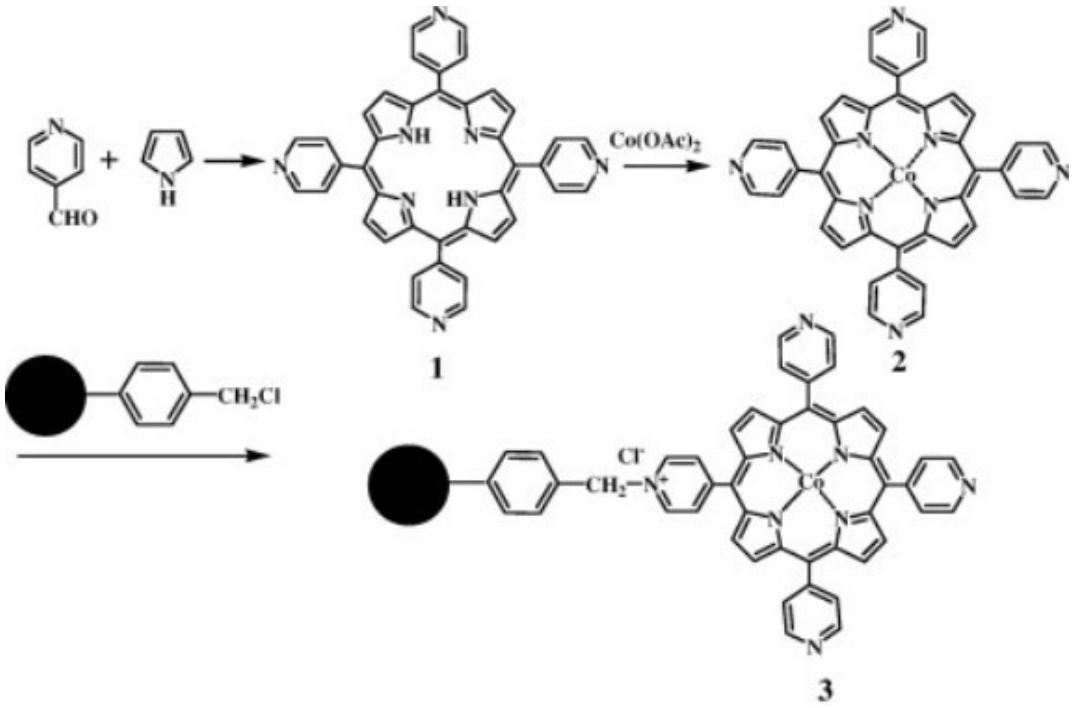

Fig 5. Schematic illustration of the preparation of Merrifield resin-Co-Py.Ref.[48]

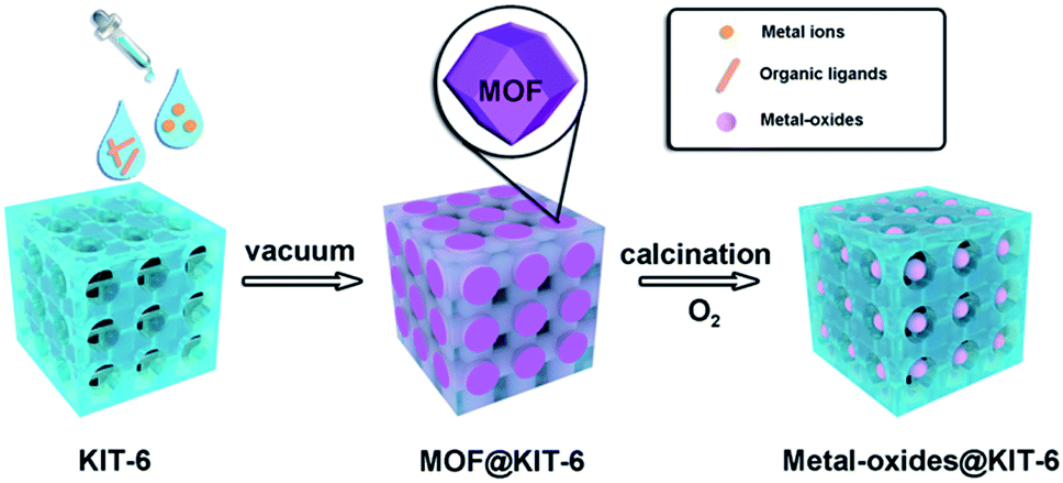

Fig 6. Synthesis route of metal-oxides@KIT-6.Ref.[49].

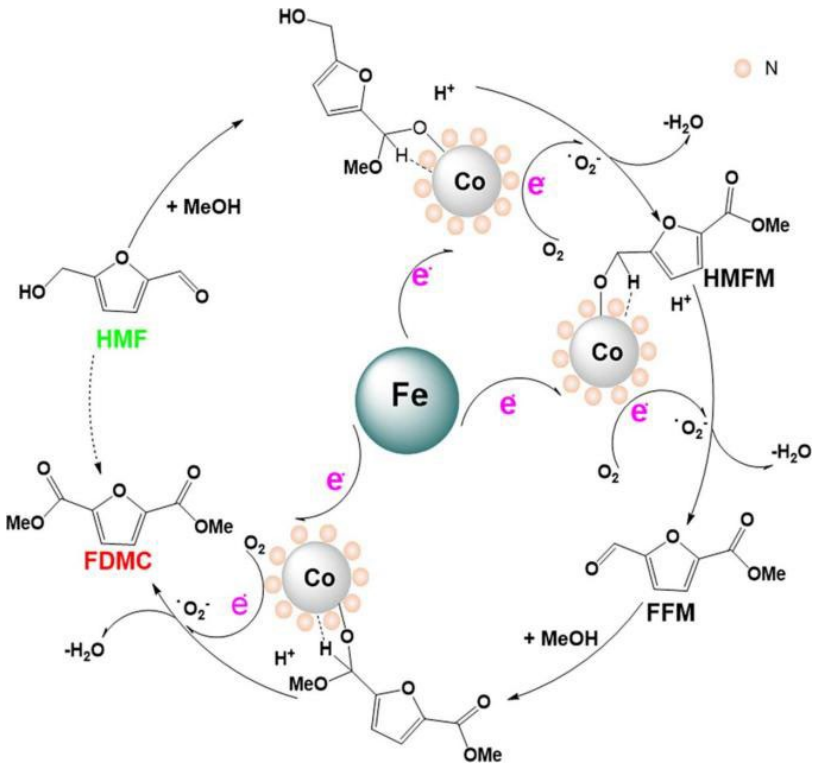

Fig 7. Probable reaction mechanism for the catalytic conversion of HMF into FDMC over Co_7Fe_3-NC.Ref.[72].

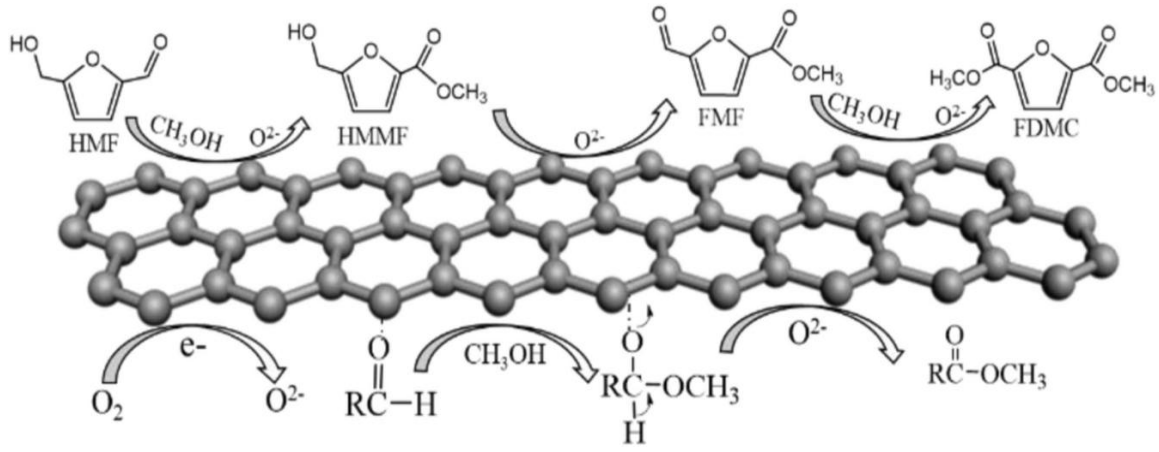

Fig 8. The reaction pathways for the conversion of HMF to FDMC.Ref.[73].

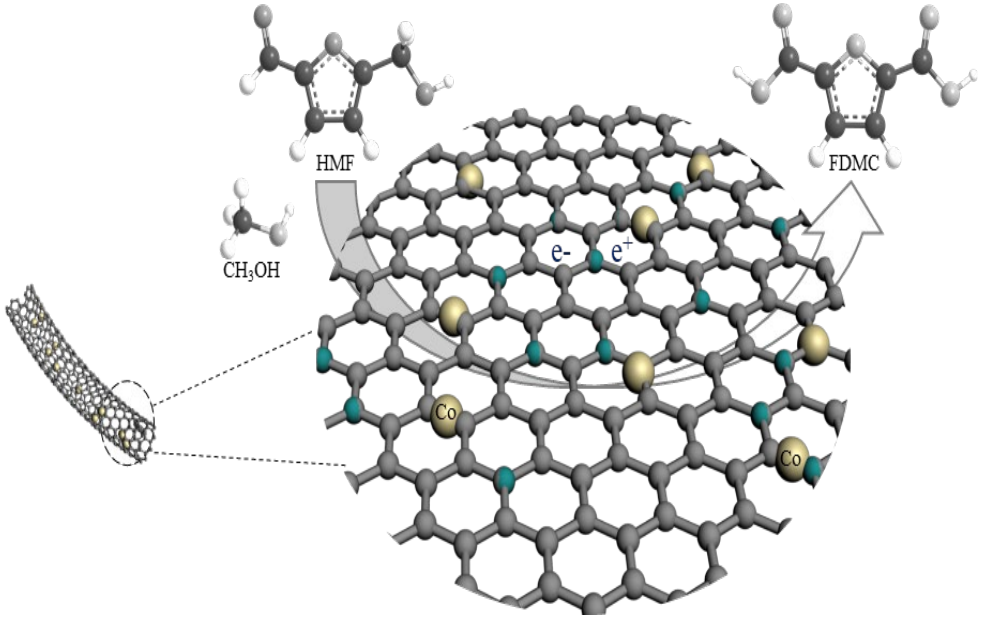

Fig 9. Co NPs loaded graphitic carbon tube catalysts involved in the methyl esterification of HMF.

Ref.[74].

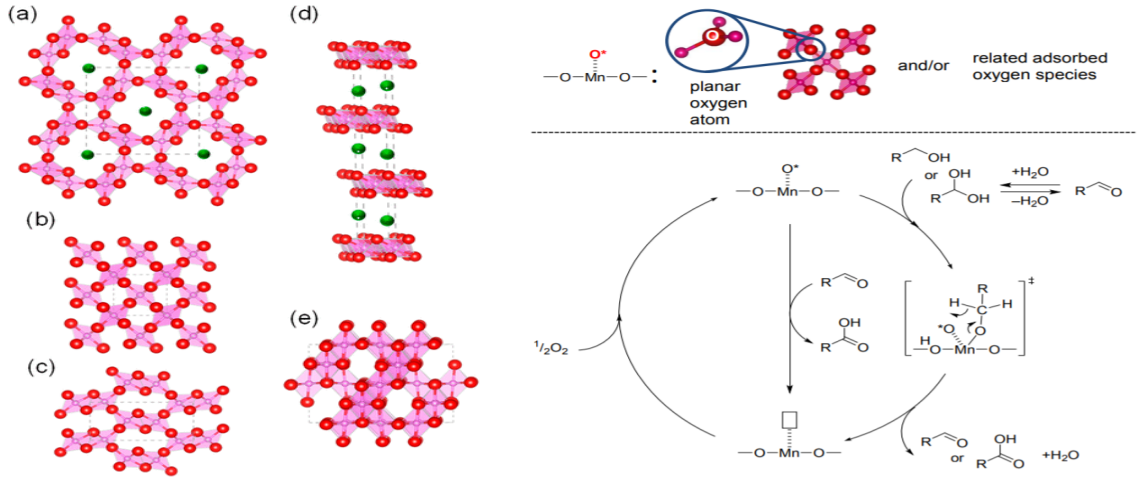

Fig 10. Structures of (a) α-MnO_2, (b) β-MnO_2, (c) γ-MnO_2, (d) δ-MnO_2, and (e) λ-MnO_2. Pink, green, and red spheres represent Mn, K, and O atoms, respectively (left).Possible reaction mechanism for the oxidation of HMF to FDCA catalyzed by β-MnO_2 (right).Ref. [90].

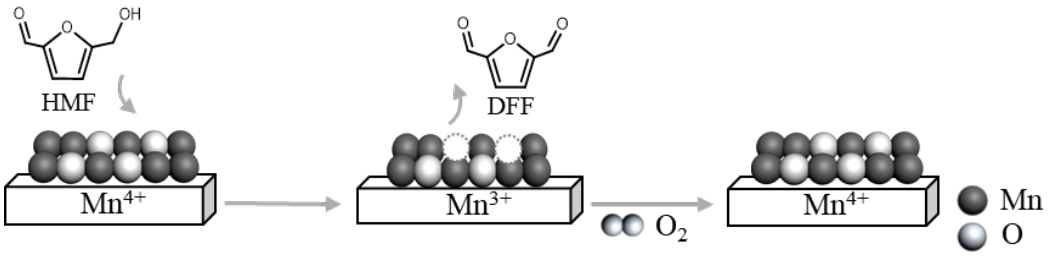

Fig 11. The reaction pathways of selective oxidation of HMF to DFF with α-MnO_2.Ref. [92].

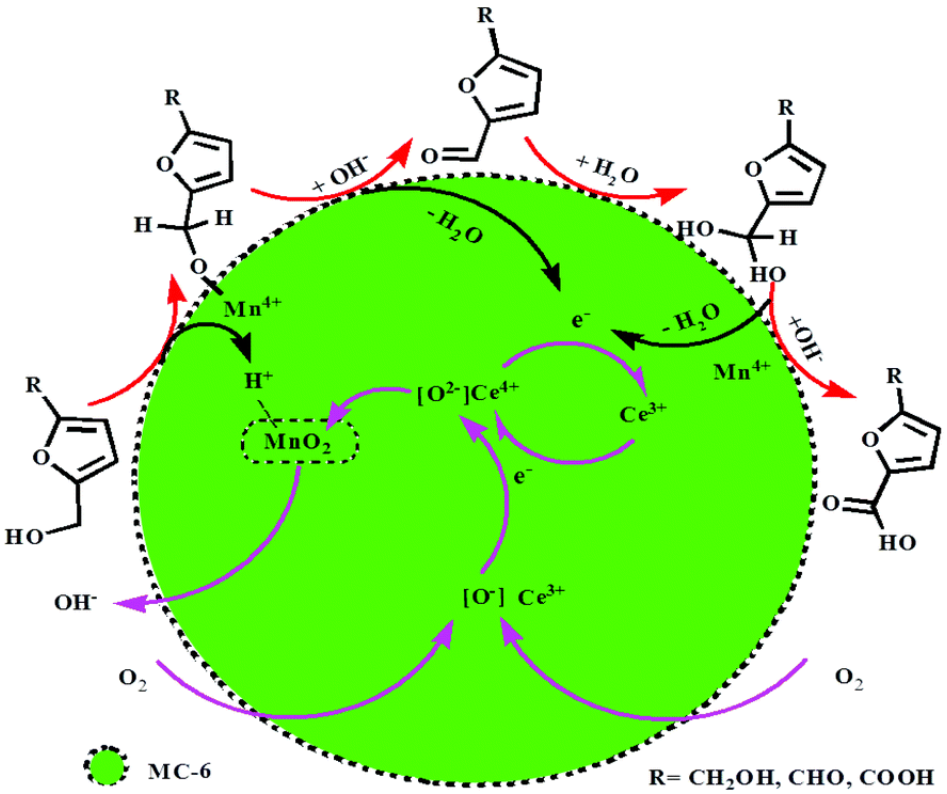

Fig 12. Reaction mechanism for the HMF oxidation over the MC-6 catalyst. Ref. [95].

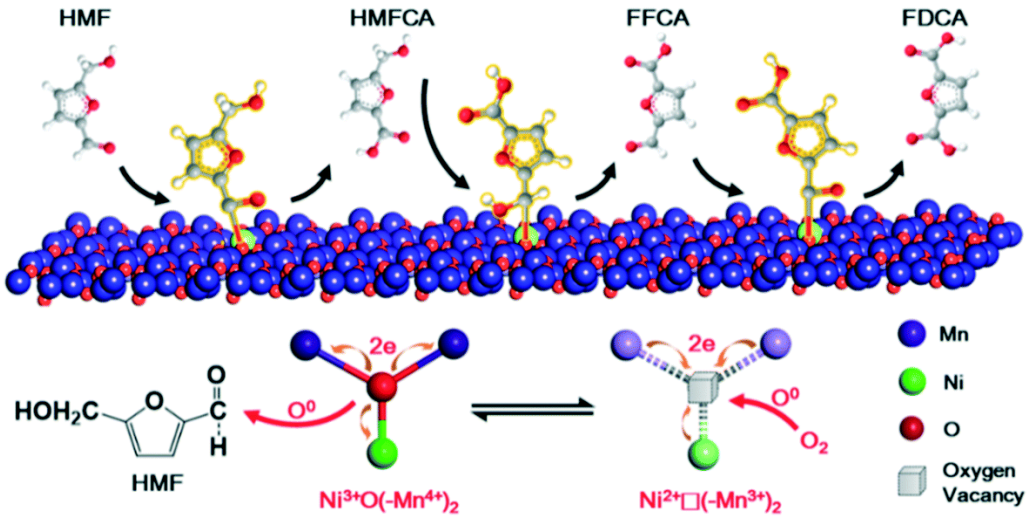

Fig 13. Top: The proposed reaction mechanism for the aerobic oxidation of HMF to FDCA on $Ni^{3+}O(–Mn^{4+})_2$ clusters in the Ni–MnO_x nanowires. Bottom: A schematic drawing to show the change from a $Ni^{3+}O(–Mn^{4+})_2$ cluster to a $Ni^{2+}□(–Mn^{3+})_2$ cluster via losing the oxygen atom and the electron transfer from the oxygen to the cations, and restoring $Ni^{3+}O(–Mn^{4+})_2$via receiving oxygen and the electron transfer from the cations to the oxygen. Ref. [102].

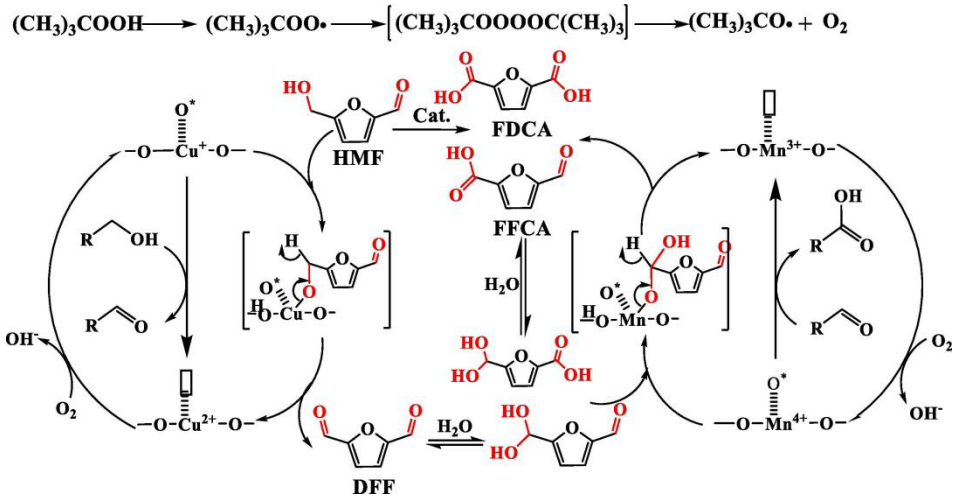

Fig 14. Possible mechanism for the oxidation of HMF to FDCA catalyzed by Cu-MnO_2@PDVTA. Ref. [113].

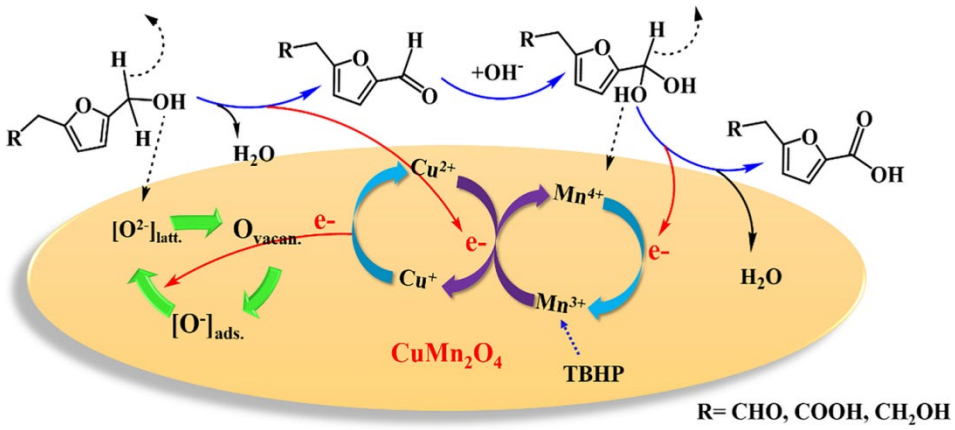

Fig 15. Possible reaction mechanism for the synthesis of FDCA from HMF over $CuMn_2O_4$ catalysts. Ref.[114].

.

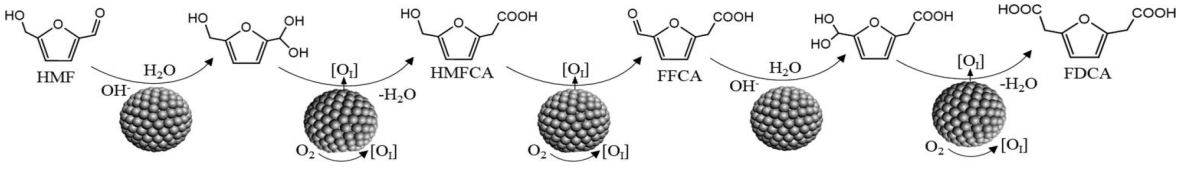

Fig 16. Proposed Reaction Pathways for Aerobic Oxidation of HMF to FDCA. Ref.[117].